Marine Micropaleontology xxx (xxxx) xxx

Contents lists available at ScienceDirect

Marine Micropaleontology

journal homepage: www.elsevier.com/locate/marmicro

Ostracod response to monsoon and OMZ variability over the past 1.2 Myr

Carlos A. Alvarez Zarikian [a,*], Chimnaz Nadiri [b], Montserrat Alonso-García [c,d,e], Teresa Rodrigues [c,d], Huai-Hsuan M. Huang [f,g], Sebastian Lindhorst [h], Tereza Kunkelova [i], Dick Kroon [j], Christian Betzler [h], Moriaki Yasuhara [f]

[a] International Ocean Discovery Program & Department of Oceanography, Texas A&M University, College Station, TX 77845, USA
[b] Department of Geology & Geophysics, Texas A&M University, College Station, TX 77845, USA
[c] Instituto Português do Mar e da Atmosfera (IPMA), Av. Alfredo Magalhães Ramalho 6, 1495-006, Lisboa, Portugal
[d] Centro de Ciências do Mar (CCMAR), Universidade do Algarve, Campus de Gambelas, 8005-139, Faro, Portugal
[e] Universidad de Salamanca, Geology Department, Pza de los Caídos s/n, 37008 Salamanca, Spain
[f] School of Biological Sciences, Area of Ecology and Biodiversity, Swire Institute of Marine Science, and State Key Laboratory of Marine Pollution, The University of Hong Kong, Pokfulam, Hong Kong, China
[g] Department of Paleobiology, National Museum of Natural History, Smithsonian Institution, Washington DC 20560, USA
[h] Institute of Geology, CEN, University of Hamburg, Bundesstraße 55, Hamburg 20146, Germany
[i] University of Southampton, National Oceanography Centre Southampton, Waterfront Campus, European Way, Southampton SO14 3ZH, UK
[j] School of GeoSciences, University of Edinburgh, Edinburgh, UK

ARTICLE INFO

Keywords:
Expedition 359
IODP Site U1467
The Maldives
Indian Ocean paleoceanography
Pleistocene
South Asian monsoon
Oxygen Minimum Zone

ABSTRACT

We present the first continuous middle through late Pleistocene record of fossil ostracods from the Maldives in the northern Indian Ocean, derived from sediment cores taken at Site U1467 by Expedition 359 of the International Ocean Discovery Program (IODP). Site U1467 lies at 487 m water depth in the Inner Sea of the Maldives archipelago, an ideal place for studying the effects of the South Asian Monsoon (SAM) system on primary productivity, intermediate depth ocean circulation, and the regional oxygen minimum zone (OMZ). The Inner Sea acts as a natural sediment trap that has undergone continuous sedimentation for millions of years with minor terrestrial influence. Our record spans from Marine Isotope Stage (MIS) 35 to the present, covering the mid-Pleistocene transition (1.2–0.6 Ma) and the Mid-Brunhes Event (MBE, at ~480 ka) the time when ice age cycles transitioned from occurring every 40,000 years to 100,000 years. The ostracod data is interpreted alongside the existing datasets from the same site of sedimentological (grain-size) and XRF-elemental analyses, and new organic biomarker data also from Site U1467. These datasets support the paleoenvironmental interpretation of the ostracod assemblages. Ostracods are abundant and diverse, displaying a prominent change in faunal composition at the MBE related to the increase in the amplitude of glacial-interglacial cycles, which deeply affected the monsoon system and thereby the past oceanographic conditions of the Maldives Inner Sea. Furthermore, ostracods exhibit distinctly different assemblages across glacial-interglacial cycles, particularly after the MBE, and these changes convincingly correspond to variability of the OMZ. Glacial periods are characterized by ostracod indicators of well-oxygenated bottom water due to the intensification of the winter monsoon and the contraction of the OMZ. Abundant psychrospheric ostracods during glacials suggests that a southern sourced water mass, such as Antarctic Intermediate Water (AAIW) and/or Subantarctic Mode water, bathed the Maldives Inner Sea during glacial periods. In contrast, interglacial stages are characterized by ostracod species and biomarker data that indicate low-oxygen conditions and sluggish bottom water circulation pointing to an expansion of the regional OMZ due to the strengthening of the summer monsoon. Our results highlight the sensitivity of ostracods to oceanographic and climate variability.

* Corresponding author.
E-mail address: zarikian@iodp.tamu.edu (C.A. Alvarez Zarikian).

https://doi.org/10.1016/j.marmicro.2022.102105
Received 16 January 2021; Received in revised form 9 February 2022; Accepted 13 February 2022
Available online 20 February 2022

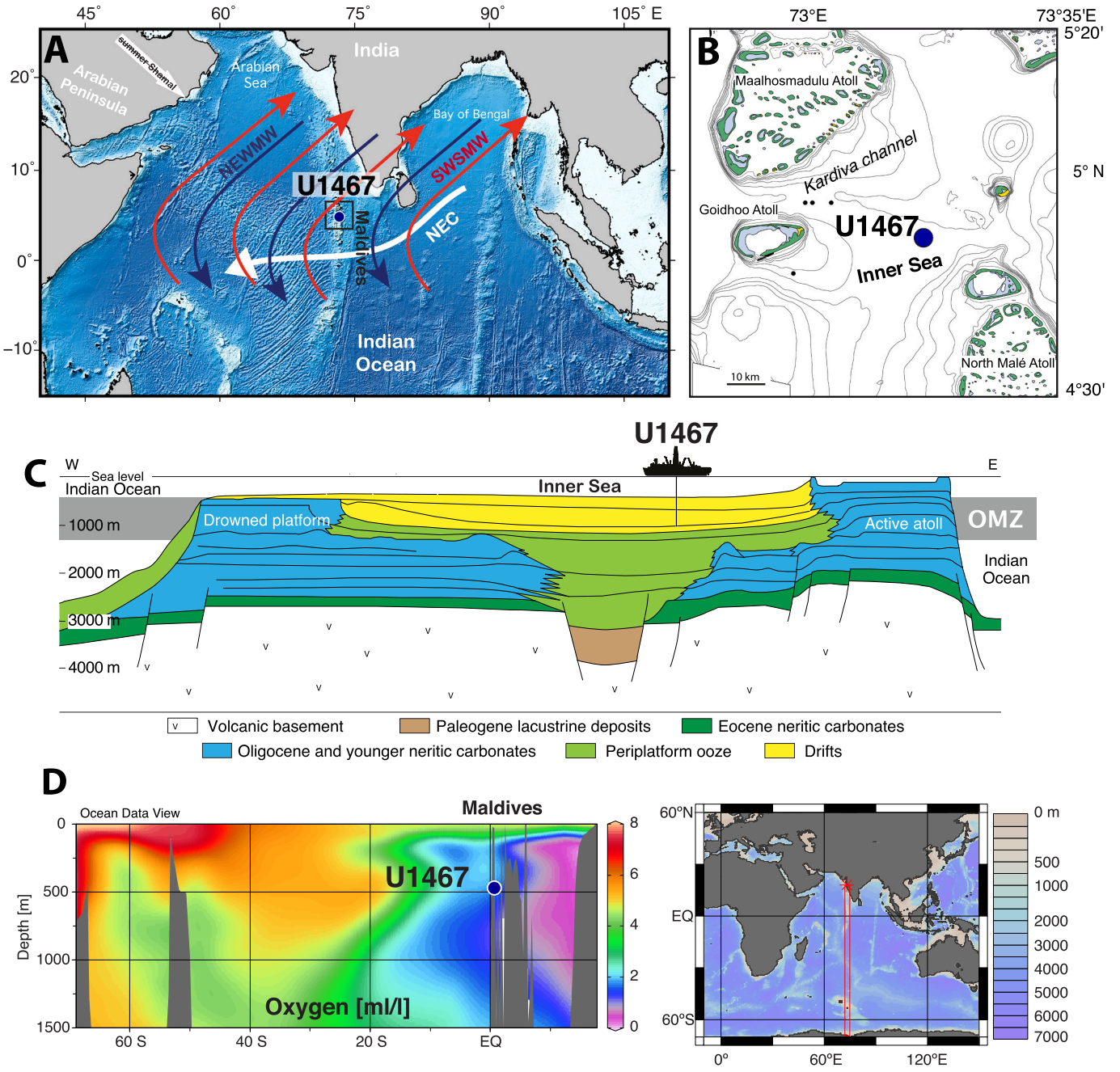

Fig. 1. Location of IODP Site U1467 (blue circle) in the Maldives, equatorial Indian Ocean. [**A**] Top left panel shows the modern monsoon wind pattern over the Arabian Sea: the northeast winter monsoon winds (NEWMW), the southwest summer monsoon winds (SWSMW), the summer Shamal winds; and the main surface current, the North Equatorial Current (NEC) during the winter monsoon (Tomczak and Godfrey, 2003). The current reverses during the summer monsoon. [**B**] Top right panel shows the bathymetric map of the Maldives Inner Sea. [**C**] The middle panel shows a schematic cross-section of the Maldives sedimentary system (adapted from Betzler et al., 2017b) with the location of Site U1467 and depth of the modern oxygen minimum zone (OMZ) in the northern Indian Ocean (horizontal gray bar). [**D**] The bottom panel shows the dissolved oxygen concentration profile across a N-S transect in the Indian Ocean [data from World Ocean Atlas 2013 (Garcia et al., 2014). (For interpretation of the references to colour in this figure legend, the reader is referred to the web version of this article.)

1. Introduction

In the equatorial Indian Ocean, the Maldives have been shaped over time by the combined effects of sea level changes, ocean circulation, and the South Asian Monsoon [SAM] (Betzler et al., 2013; Lüdmann et al., 2013). The SAM is an important climatic system that drives seasonal reversals in atmospheric and oceanic circulation which controls the biological productivity in the northern Indian Ocean by inducing upwelling in different regions depending on the wind direction (Tomczak and Godfrey, 2003). During the summer monsoon (June to September), southwesterly winds bring strong precipitation over southern Asia and promote the flow of the Southwest Monsoon Current along the northern and central Indian Ocean. This drives intense upwelling and primary productivity changes in the western Arabian Sea (Wyrtki, 1973; Nair et al., 1989; Schulte et al., 1999). Present-day primary productivity in the Maldives peaks in September, at the end of the summer monsoon season, but it is moderate compared to high productivity areas of the Arabian Sea upwelling regions (Antoine et al., 1996). The upwelling effect in primary productivity is reduced by the formation of a low salinity surface layer that results from local summer rainfall and the

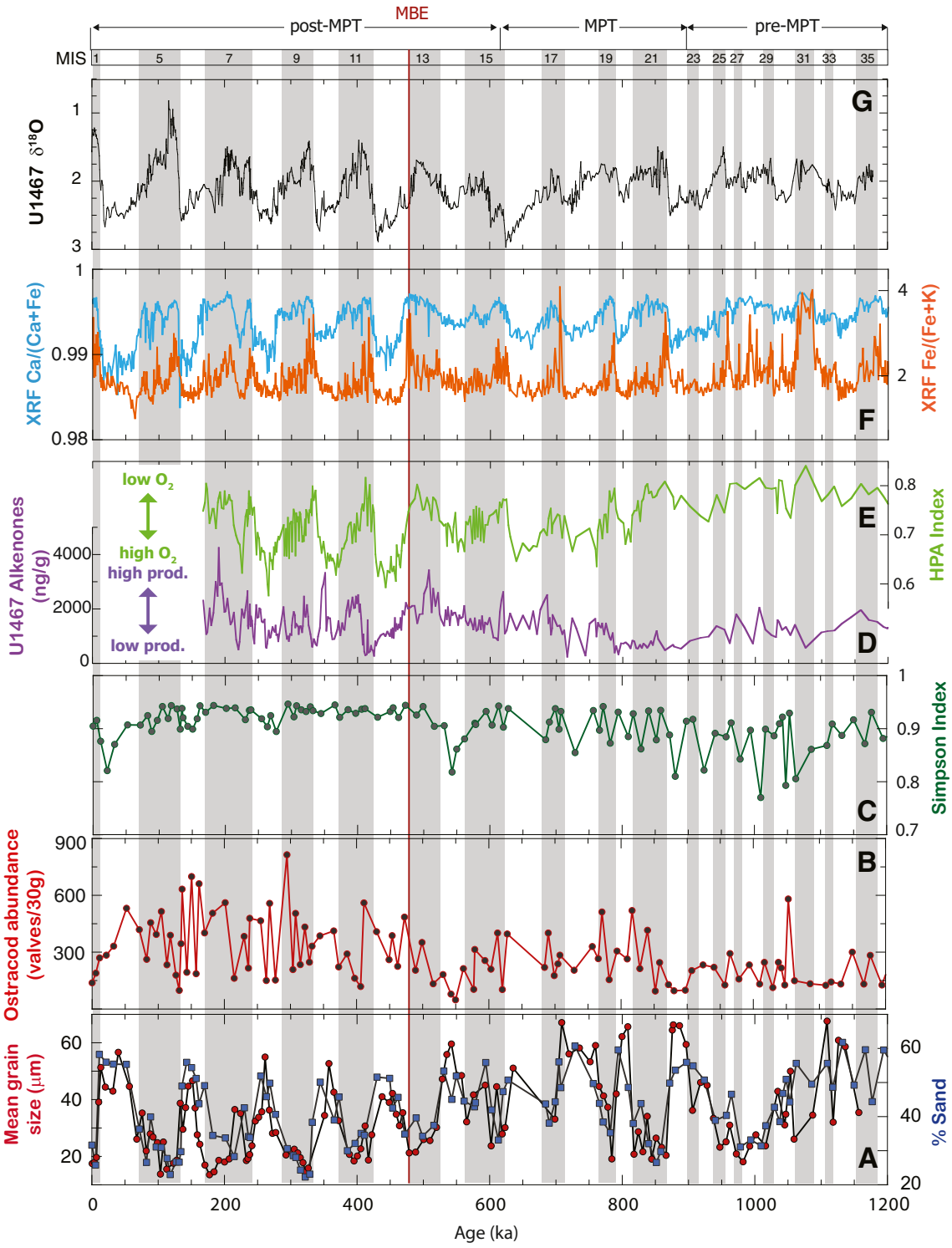

Fig. 2. From bottom to top: **A**) Results of grain-size analyses of the Site U1467 sediments: bulk sediment mean grain size (μm, dark red circles) and the proportion (%) of sand fraction (>63 μm) in the samples analyzed for ostracods (blue squares); **B**) total ostracod abundance (number of valves per 30 g of sediment; dark red line); **C**) ostracod diversity expressed by the Simpson index (dark green line); **D**) total alkenone concentration (ng/g; purple line), from Alonso-Garcia et al. (2019) and this study; **E**) the higher plant n-alcohols/n-alkanes (HPA) ventilation index (green line); **F**) XRF derived elemental ratios of Ca/Fe (light blue line) and Fe/K (orange line) of the sediment cores from Site U1467; and **G**) the Site U1467 benthic $\delta^{18}O$ record from Stainbank et al. (2020) measured on the benthic foraminifer *Cibicides mabahethi*. The HPA index indicates the degree of organic matter preservation, and therefore oxygenation, on the seafloor, and the total alkenone concentration sea surface primary productivity (Alonso-Garcia et al., 2019). No biomarker data is available for MIS 1–6. The Ca/Fe records variations between continental aelioan dust input and in-situ carbonate production. The terrigenous element ratio of Fe/K indicate variations in dust input during winter monsoon (Kunkelova et al., 2018). Interglacial Marine Isotope Stages (MIS) are highlighted by gray bars. The Mid-Brunhes event (MBE) is marked by the vertical dark red line at ~480 kyr. The MBE marks the increase in amplitude of glacial-interglacial cycles at the transition between MIS 13 and 12. (For interpretation of the references to colour in this figure legend, the reader is referred to the web version of this article.)

inflow of low salinity waters from the Bay of Bengal (Schulte et al., 1999). The formation of a low salinity layer creates strong stratification of the water column, reducing ventilation, and regulating the Indian Ocean oxygen minimum zone (OMZ), which is considered one of the largest in the world (Lachkar et al., 2018). During winter months (November–April), northeasterly winds intensify promoting arid conditions over southern Asia (Kunkelova et al., 2018), and the flow of the North Equatorial current westwards (Wyrtki, 1973; Betzler et al., 2016). Because of its location in the central equatorial Indian Ocean (Fig. 1), the Maldives is an ideal region for exploring the monsoon system and its effects on primary productivity, ocean currents, and bottom water ventilation related to the OMZ.

In 2015, the International Ocean Discovery Program (IODP) Expedition 359 drilled eight sites (U1465-U1472) aligned in two east-west transects north and south of the Goidhoo atoll in and across the central part of the Maldives carbonate edifice at water depths from 379 m to 521 m and recovered shallow water carbonate platform to deep water carbonate drift deposits that revealed a nearly complete Cenozoic carbonate sedimentary record of the Maldives (Betzler et al., 2017a). Here, we examine fossil ostracods, minute benthic microcrustaceans that secrete a bivalved calcareous carapace, obtained from cores taken at Site U1467 to reconstruct the history of bottom water ventilation and effects of the regional OMZ related to Monsoon dynamics on primary productivity, intermediate depth ocean circulation over the past 1.2 Myr. We analyze our ostracod dataset in combination with petrophysical and biogeochemical proxies that include X-ray fluorescence core scanning, biomarkers, and sediment grain size derived from Site U1467. The time interval studied includes two outstanding climate transitions, the mid-Pleistocene transition (MPT, 1.2–0.6 Ma) and the Mid-Brunhes Event (MBE, ~480 ka). During the MPT, the Earth's climate shifted from glacial-interglacial cycles of 41,000 years to 100,000 years cyclicity (Pisias and Moore Jr., 1981), whereas at the MBE the amplitude of the glacial interglacial cycles increased with warmer interglacial periods after MIS 11 (Jansen et al., 1986). The South Asian monsoon also was strongly impacted by the MBE through the strengthening of the winter monsoon (Kunkelova et al., 2018).

1.1. Ostracods in the Indian Ocean and the Maldives

Ostracods have been comparatively less studied in the Indian Ocean than in other oceans around the world. Most Indian Ocean studies focus on modern shallow to bathyal marine faunas along the Indian coast in the Bay of Bengal and the Arabian Sea (Jain, 1981; Hussain, 1998; Sridhar et al., 2002; Hussain et al., 2004, 2007; Gopalakrishna et al., 2007, 2008; Mostafawi et al., 2010; Munef et al., 2012; Iwatani et al., 2014; Nishath et al., 2015, 2017), from the Persian Gulf to the Mozambique channel (Maddocks, 1966, 1969a, 1969b; Bonaduce et al., 1976, 1980; Malz and Jellinek, 1989; Jellinek, 1993; Babinot and Kouyoumontzakis, 1995; Mostafawi, 2003; Mohammed and Keyser, 2012; Mohammed et al., 2012), and from the Malaysia-Indonesia region (Kingma, 1948; Whatley and Zhao, 1987, 1988; Dewi, 1993; Zhao and Whatley, 1997; Mostafawi et al., 2005; Fauzielly et al., 2013; Iwatani et al., 2018; Shin et al., 2019). Only a few regional stratigraphic studies on late Cenozoic ostracods have been published to date (Benson, 1974; Guernet, 1993; Yasuhara et al., 2017; Shin et al., 2019), and even fewer have been published from the Maldives. The few that exist are primarily about single species taxonomic descriptions (Maddocks and Wouters, 1990; Wouters, 1996, 1997, 2004). The present study provides the first comprehensive examination and documentation of Pleistocene ostracods from the Maldives to date.

1.2. Geological setting

The Maldives Inner Sea is a small, perched basin, elevated in relation to the Indian Ocean and surrounded by atolls that lie near or slightly above the sea surface in the large and elongate isolated tropical archipelago of the Maldives located southwest of India in the northern Indian Ocean. The maximum water depth of this inter-atoll sea is 550 m. The Maldives carbonate edifice has been developed since the Eocene on the volcanic rocks of the Chagos-Laccadives Ridge. The discontinuous marginal rim of the Inner Sea is formed by small atolls with 50–60 m deep lagoons. The atoll's rims are cut by deep passages where strong currents flow between the lagoons and the open sea allowing subsequent sediment reworking and re-deposition (Ciarapica and Passeri, 1993; Betzler et al., 2015). The external slopes of the platform margin toward the ocean are very steep, rapidly reaching the bathyal and abyssal depths of the Indian Ocean (Lüdmann et al., 2013). Far away, and isolated from India and Asia, the Maldives has grown to a ~ 3 km thick carbonate sedimentary succession that embodies an almost complete Cenozoic sedimentary record with minimal terrigenous input (Aubert and Droxler, 1992; Purdy and Bertram, 1993; Lüdmann et al., 2013; Lindhorst et al., 2019). Seismic data at the location of Site U1467 show a broad, shallow basin with nearly horizontally layered seismic reflections (Betzler et al., 2013, 2017b; Lüdmann et al., 2013). All these characteristics make the Maldives Inner Sea a natural sediment trap. Results from shipboard measurements conducted during Expedition 359 showed that the sediments obtained at Site U1467 consist of hundreds of meters of unlithified foraminifera-rich mudstone, wackestone to packstone, with abundant and well-preserved calcareous microfossils (Betzler et al., 2017b). The site's nannofossil and planktonic foraminiferal biostratigraphy suggest a continuous, complete and undisturbed stratigraphic succession of sheeted drift deposits extending back to the middle Miocene that provides a mostly unread sedimentary archive of past oceanographic and climatic changes spanning millions of years (Betzler et al., 2016, 2017b, 2018; Kunkelova et al., 2018).

2. Materials and methods

2.1. IODP Site U1467

This study uses core samples from IODP Site U1467 (4°51.031′N, 73°17.020′E) cored at a water depth of 487 m in a central position in the Maldives Inner Sea (Fig. 1). Four holes were cored at the site for the purpose of recovering stratigraphic sections suitable for building a complete composite section of the Plio-Pleistocene hemipelagic carbonate drift succession. One hole (U1467C) was deepened to 714 m below the seafloor (mbsf) to reach the base of the drift deposits, which expanded the site's record to the middle Miocene (Betzler et al., 2017b). The composite core depth below the seafloor (CCSF) or *splice* of Site U1467 is based on the stratigraphic correlation of sediment physical and magnetic properties of cores retrieved from Holes U1467B and U1467C (Betzler et al., 2017b), and later refined onshore by correlating X-Ray Fluorescence (XRF) core scanning data from these holes (Kunkelova et al., 2018).

2.2. The age model

We use the age model from Alonso-Garcia et al. (2019) which is consistent with the age model of Stainbank et al. (2020) based on the newly produced planktic and benthic foraminifer $\delta^{18}O$ records from Site U1467 correlated to the global stack reference curve of Ahn et al. (2017). The benthic $\delta^{18}O$ record derived from the benthic foraminifer *Cibicides mabahethi* is shown in Fig. 2. Ma. Based on the age model, the 40 m composite core record studied here extends from the present day back to ~1.2 Ma, providing an average sedimentation rate of 3 cm/kyr.

2.3. Ostracod analyses

Ostracod analyses were performed on the size fraction larger than 150 μm of 109 sediment core samples. Each sample had a thickness of 2 cm and a volume of ~35 cm^3, and were taken at 40 cm intervals over the core composite depth interval of 0 to 40 m below the seafloor. At 3 cm/

kyr sedimentation rate, the 40-cm sample spacing provides an average sample resolution of ~12 kyr and each 2-cm sample represents the integrated sedimentation over a period of ~666 yrs. Before sample processing, we first freeze-dried them and measured their bulk weight, wet-sieved them using a 63-μm mesh, oven-dried them at ~40 °C, and finally weighed the sand fractions. For ostracod characterization, we dry-sieved the samples and picked all the ostracods present in the >150 μm grain size fraction of the dried residues using a Zeiss Stemi SV11 stereoscope. We counted all complete or minimally broken ostracod valves and carapaces and counted one left or right valve and one articulated carapace (= two articulated valves) as one and two ostracods, respectively. We digitally imaged adult and juvenile specimens of most taxa with an FEI Quanta 600 FE scanning electron microscope at Texas A&M University to aid with the identification and documentation of the taxa. We identified ostracods to genus level and when possible to species level following mainly the taxonomy of Hartmann, 1964, 1974Hartmann-Schröder and Hartmann (1978), Bonaduce et al. (1976, 1980), Whatley and Zhao (1987, 1988), Zhao and Whatley (1989), Howe and McKenzie (1989), Whatley and Keeler (1989), Mostafawi (1992), Jellinek (1993), Titterton and Whatley (1988, 2005, 2006a, 2006b, 2007, 2008a, 2008b) and Munef et al. (2012). We inferred ostracod habitats from the modern ecology of related genera (Elofson, 1941; Maddocks, 1969a, 1969b; Bonaduce et al., 1976; Jellinek, 1993; Majoran and Agrenius, 1995; Ikeya and Kato, 2000; Gopalakrishna et al., 2007, 2008; Jöst et al., 2018; Hong et al., 2019) and based on paleoecological interpretations by previous works on late Cenozoic ostracods (e.g., Yasuhara and Cronin, 2008; Yasuhara et al., 2008, 2017; Alvarez Zarikian et al., 2009; Iwatani et al., 2018; Shin et al., 2019).

2.4. Statistical analyses of the ostracod data

We analyzed the ostracod assemblage data using community-scale statistics that include the number of ostracod specimens standardized to an average sample weight of 30 g, relative abundance (%) and average frequency of individual genera, the number of taxa per sample (richness), the Simpson index, Non-Metric Multidimensional Scaling (NMDS), Q-mode k-means clustering, and Genera Indicator Value. The average frequency equals ΣPi/n, where Pi is the relative percentage of the species in each sample, and n is the total sample number. We use the Simpson index to evaluate the taxonomic diversity of each sample because this method has been shown to be useful in ostracod studies because it is relatively insensitive to sample size (Magurran, 2003; Morris et al., 2014; Huang et al., 2018). Its calculation follows Simpson (1949): $1–\Sigma Pi^2$, where Pi is relative percentage of a species.

We applied NMDS, Q-mode k-means clustering, and Indicator Value analysis to the data. All samples were included in the statistical analyses using generic relative abundances (%). The NMDS is a statistical ordination method that takes into account taxonomic composition and abundance to produce ordinations of the assemblage data. When one compares the taxonomic compositions of assemblages among samples, there would be as many dimensions as the number of taxa. To reduce the number of dimensions and to understand the most important relationship among assemblages, we used the NMDS to preserve the ranking relationship among samples in a two-dimensional plot (Borcard et al., 2011; Legendre and Legendre, 2012). Conducting the NMDS on the assemblage data in the R package "vegan" (Oksanen et al., 2018), we applied Bray-Curtis dissimilarity as the distance metric. Samples with more different taxonomic compositions or relative abundances of different taxa would be farther away from each other in an NMDS plot. For the NMDS, we used all 109 samples and the relative abundances of all genera. Note that the axes in the NMDS plot could be arbitrarily rotated, for example, being positive or negative has no ecological meaning. However, both axes (NMDS1 and NMDS2) indicate important signals of change in the faunal composition.

Q-mode k-means clustering divides the samples into a given number of clusters, minimizing the compositional difference within clusters by iteratively minimizing the sum of the sums of the squared distances among samples within each cluster (Borcard et al., 2011). We conducted the k-means clustering on the NMDS scores of samples in the R package "stats" (R Core Team, 2017). We used Simple Structure Index as the criterion for determining a suitable number of clusters, i.e., achieving the most contrasting groups (Borcard et al., 2011; 3 clusters in this case). We then used the Indicator Value Analysis along with permutation testing to determine the significant genus indicators for each cluster (Dufrêne and Legendre, 1997). For the calculation of the indicator values, we used a subset of the data where rare genera, those with less than 100 total number of specimens, were excluded. Eventually, 30 genera were included in the Indicator Value Analysis done in the R package "labdsv" (Roberts, 2019). A significant indicator (i.e., p-value <0.05) was determined by having a high indicator value for a cluster where it more exclusively occurs with high frequency and high relative abundances (Dufrêne and Legendre, 1997).

2.5. Sedimentological analyses

In addition to calculating the sand content of the samples analyzed for ostracods, we integrated into our record bulk grain size measurements of 150 additional samples taken at 25 cm intervals over the same stratigraphic interval at Site U1467. These samples were measured with a Sympatec Helos KFMagic laser particle-size analyzer and a measuring range of 0.5/18–3500 μm at the University of Hamburg, Germany (for complete methodology see Lindhorst et al., 2019). These samples were wet sieved using a 2000 μm mesh prior to the grain-size measurements to remove very coarse particles (for example coral detritus and large pteropod shells). All samples were dispersed in water using ultrasonic and 0.05% $Na_4P_2O_7$ x 10 H_2O (tetra-sodium diphosphate decahydrate) as dispersing agent. To ensure accuracy of the measurements and absence of long-term instrumental drift, an in-house grain-size standard was measured daily prior to a series of measurements (standard deviation was <3.3 μm for 0.5/18–3500 μm). Grain-size statistics are based on the graphical method (Folk and Ward, 1957) and were calculated using Gradistat (Blott and Pye, 2001). Values for percentages are rounded to the nearest integer.

2.6. X-ray fluorescence (XRF) core scanning

We compared the downcore ostracod data to element ratios of Ca/Fe and Fe/K derived from non-destructive X-ray fluorescence (XRF) scanning of the sediment cores. The cores were measured at the International Ocean Discovery Program's Gulf Coast Repository (GCR) in College Station, Texas (USA) using a third generation AvaaTech XRF scanner configured to analyze split sediment core halves for elements between Mg and U in the periodic table (Backman and Lyle, 2013). The data were acquired with a Canberra X-PIPS Silicon Drift Detector (SDD) with 150 eV X-ray resolution at 5.9 keV and a Canberra Digital Spectrum Analyzer model DAS 1000. The X-ray source was an Oxford Instruments 100 W Neptune X-ray tube with a rhodium (Rh) target. Raw spectral data were processed using the Canberra WINAXIL software package to produce elemental intensity data. The dual slit system was set to provide downcore spatial resolution of 10 mm and cross-core spatial resolution of 12 mm. The system was set to perform two consecutive runs of the same section, the first one at 9 kV, 0.25 mA and 6 s, and the second one at 30 kV, 1.25 mA and 6 s. The first scan provides data for the elements Mg, Al, Si, S, P, Cl, Ar, K, Ca, Ti, Cr, Mn, Fe, Rh and Ba, and the second for Fe, Ni, Cu, Zn, Ga, Br, Rb, Sr, Y, Zr, Nb, Mo, Pb, and Bi. Each core section was removed from refrigeration at least 2 h before scanning and scraped to clean and smooth the core surface. The split core surface was covered with 4 μm thick Ultralene plastic film to prevent contamination of the X-ray detector. Measurements were taken at 3 cm intervals except when sediment cracks or uneven surfaces forced us to skip or shift the measurement to the nearest suitable area. To evaluate the reliability of the analysis of certain elements (Fe, Al, Sr, Si K, Ca, Br, Mo, and Ba) an

associated study (Kunkelova et al., 2018) analyzed samples of pressed pellets using a fully quantitative conventional XRF method. That study measured 67 samples from Cores 359-U1467C-4H to —6H on a conventional XRF instrument in Edinburgh with the same pellets measured on the AvaaTech XRF core scanner in College Station, Texas. For the detailed methodology please refer to Kunkelova et al. (2018). The Ca, Fe, and K data are in counts per second. The XRF measurements were normalized dividing the raw total counts of each element by the total counts for each measurement excluding Ag and Rh to reduce the effects of water content, porosity and lithological variability (Tjallingii et al., 2007; Kunkelova et al., 2018).

2.7. Organic compounds

The total concentration of *n*-alkanes, *n*-alkan-1-ols and C_{37} alkenones were measured in 350 samples from Site U1467 for the interval from Marine Isotope Stage (MIS) 35 to 7 (~1200–175 ka; Fig. 2). Unfortunately, measurements for the interval from 175 ka to the present were not finalized by the time we wrote this manuscript. The organic biomarkers were extracted from the sediments and analyzed as described in Villanueva et al. (1997) in the laboratories of IPMA (Lisbon, Portugal). Sediment samples were freeze-dried and the organic compounds were extracted by sonication using dichloromethane. The extracts were digested with 6% potassium hydroxide in methanol to eliminate interferences from wax esters, proteins, and other hydrolysable compounds. The neutral lipids were extracted with hexane, evaporated to near dryness under a N_2 stream and finally derivatized with bis(trimethylsilyl)trifluoroacetamide. The extracted compounds were identified with a Bruker mass spectrometer detector and quantified with a Varian gas chromatograph Model 3800 equipped with a septum programmable injector and a flame ionization detector with a CPSIL-5 CB column. We used hydrogen as a carrier gas at a flow rate of 2.5 ml/min. The chromatograms were processed with the Galaxie software and concentrations were determined using n-hexatriacontane as an internal standard.

The total concentration of *n*-alkanes and C_{37} alkenones for the interval from MIS 14 to 7 was already published in Alonso-Garcia et al. (2019). In that study, C_{37} alkenone concentration was interpreted as a proxy to infer surface water productivity related to coccolithophores, and selected *n*-alkanes and *n*-alcohols were interpreted as a proxy for hydrological balance in the nearby continents, given that long-chain *n*-alkanes and n-alcohols are organic compounds that reflect continental input because they come from epicuticular leaf waxes of higher plants (Poynter and Eglinton, 1990; Poynter et al., 1989). In this study, *n*-alkanes and *n*-alkan-1-ols were identified and quantified in order to calculate the Higher Plant *n*-alcohols/(*n*-alcohols + *n*-alkanes) (HPA) index. We used the equation proposed by Poynter and Eglinton (1991), HPA = 24–28-OH/(24–28-OH + C27–31), in which the concentration of *n*-alkan-1-ols with 24, 26 and 28 carbon atoms is compared to *n*-alkanes with 27, 29 and 31 carbon atoms. The HPA index (or similar ratios between the *n*-alkan-1-ols and the *n*-alkanes) has been widely applied to evaluate changes in bottom water oxygenation in sedimentary records, i.e., ventilation and organic matter preservation, since both compounds have the same source and the *n*-alkan-1-ol compounds are prone to degradation whereas the *n*-alkanes are more resistant compounds (Bogus et al., 2012; Cacho et al., 2000; Rodrigues et al., 2011; Westerhausen et al., 1993). In well-oxygenated waters the concentration of *n*-alkan-1-ol compounds decreases and, therefore, the HPA index would show low values.

3. Results and discussion

3.1. Sediment composition, grain size, and biomarkers

Site U1467 was cored in carbonate drift deposits consisting of periplatform ooze formed through off-bank transport of carbonate particles from the shallow water carbonate factories and pelagic carbonate- and silica production (Betzler et al., 2017b; Lindhorst et al., 2019). The bulk grain size data reflect varying input from these sources. Previous studies have shown a general fining of carbonate drift sediments during sea-level highstands when export of mud size particles from shallow water banks and atolls is at its maximum (Schlager et al., 1994; Betzler et al., 2013). By contrast, sediment coarsening occurs when sea level is low, banks and atolls emerge, and likely bottom water circulation becomes more vigorous, which would enhance ventilation at the seafloor.

The sediment samples from Site U1467 consist of calcareous microfossil ooze. The sand fraction contains predominantly well-preserved planktonic foraminifers, but also ostracods, benthic foraminifers, pteropods, mollusk and echinoid fragments, and dark brown organic matter. The bulk sample grain size mean varies from 14 to 68 μm, and averages 33 μm. Mud content (sediment grain size <63 μm) ranges from 47 to 91%, with a median of 69%, indicating that the samples are mainly composed of silt and clay. Grain size profiles show temporal oscillations that effectively follow glacial/interglacial cyclicity, with coarser sediment in glacial intervals, and finer grain size content in interglacial periods (Fig. 2).

Overall, total alkenone concentrations at Site U1467 increase over time and show higher variability toward the late Pleistocene (Fig. 2). Superimposed on this trend are two main periods of reduced concentrations, one from MIS 24 through MIS 22 and another one across MIS 12. Thereafter, total alkenone concentrations show high amplitude fluctuations throughout the late Pleistocene. Alonso-Garcia et al. (2019) interpreted these changes as variations in surface productivity in the Maldives related to intensification of the Indian Ocean Equatorial Westerlies (IEW), with periods of elevated alkenone concentrations linked to increased productivity. The HPA index (Fig. 2) reflects bottom water oxygenation in the Maldives Inner Sea, which is linked to the OMZ in the northern Indian Ocean. Enhanced summer monsoon conditions intensify productivity in the Arabian Sea and expand the OMZ (Lachkar et al., 2018), therefore, variations in the HPA index may reflect past contractions and expansions of the OMZ. Our record shows a trend from high values and low variability in the earlier part of the middle Pleistocene to lower values and high variability in late Pleistocene. High values (low bottom water oxygenation) prevail between MIS 35 through MIS 25. This period is followed by a trend of decreasing values through MIS 16 marked by sharp episodic increases in the HPA index coincident with interglacial stages. In contrast, high HPA values are recorded during MIS 15–13. Beginning in MIS 12, high amplitude variability reflects alternating low (high bottom water oxygenation) and high (reduced ventilation) values during glacial and interglacials, respectively. Although no biomarker data are available for the period between MIS 6 and 1, the existing record points to similar glacial-interglacial oscillations for the latest part of the record in the HPA index and the total alkenone concentration.

3.2. Elemental records from XRF core scanning

The Ca/Fe and Fe/K records show temporal variability in lithogenic and biogenic sediment components that is synchronous with the glacial-interglacial cyclicity dominating the climate system over the last 1.2 Myr (Fig. 2). The Ca/Fe ratio represents variations between biogenic carbonate production versus eolian input and shows higher Fe (dust input) during glacials and higher Ca (biogenic carbonate production) during interglacials (Kunkelova et al., 2018). Ca is normalized to Fe as terrestrial sources are considered the principal source of Fe to the open ocean in the northwest Indian Ocean (León and Legrand, 2003). On the other hand, variability in the lithogenic components (Fe/K ratio) of the carbonate drift sediments in the Maldives Inner Sea has been linked to precipitation changes in the dust source areas that are controlled by the monsoonal system (Bunzel et al., 2017; Kunkelova et al., 2018). During interglacial periods, stronger summer monsoon (winds from the SW, Fig. 1) creates more humid conditions over India that result in intensification of rain and chemical weathering and increased fluvial material

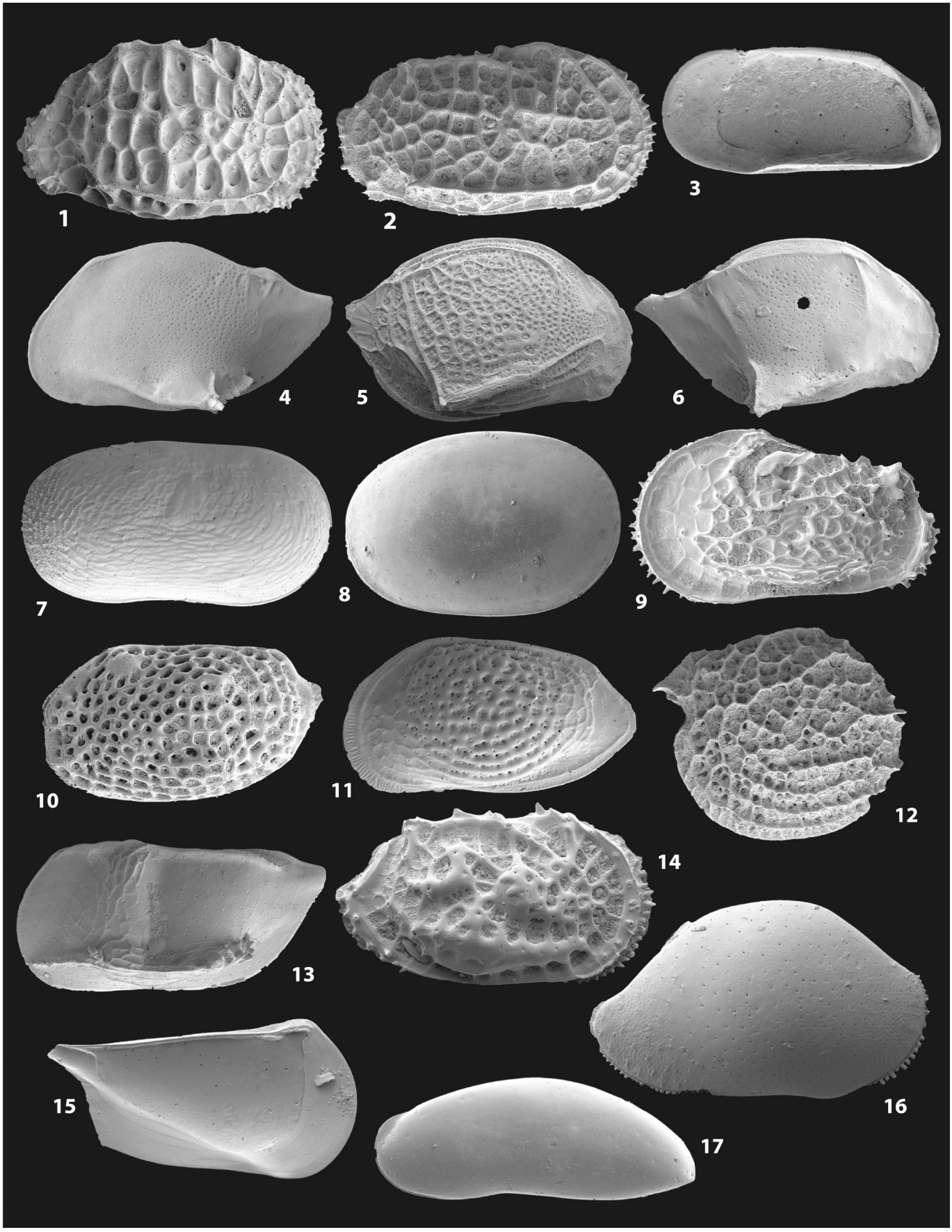

(caption on next page)

Fig. 3. Common ostracods at IODP Site U1467, in the Maldives. **1**) *Bradleya* sp. A (RV, length: 895 μm). **2**) *Bradleya thomasi* Steineck and Yozzo, 1988 (RV, 1020 μm). **3**) *Krithe dolichodeira* van den Bold 1946 (RV, 744 μm). **4**) *Cytheropteron haoae* Zhao, Whatley, and Zhou 2000 (RV, 760 μm). **5**) *Cytheropteron* aff. *C. hadriaticum* Bonaduce, Campo, and Masoli 1975 (RV, 464 μm). **6**) *Cytheropteron* cf. *C. excisum* Bonaduce, Masoli, and Pugliese, 1976, (RV, 530 μm). **7**) *Cytherella dictyon* Malz and Jellinek, 1989 (RV, 875 μm). **8**) *Cytherella* cf. *lata* Kingma, 1948, (RV 890 μm). **9.** *Stigmatocythere* sp. (RV, 545 μm). **10**) *Loxoconcha ghardaqensis* Hartmann, 1964 (LV, 481 μm). **11**) *Palmoconcha* sp. (LV, 536 μm). **12**) *Polycope* aff. *P. clathrata* Sars, 1923 (LV, 470 μm). **13**) *Bythoceratina paiki* Whatley and Zhao, 1987, (LV, 970 μm). **14**) *Agrenocythere* sp. (RV, 970 μm). **15**) *Pseudocythere* sp. (LV, 600 μm). **16**) *Paranesidea* sp., (RV, 1100 μm). **17**) *Argilloecia acuminata* G.W. Müller, 1894 (LV, 540 μm). RV: right valve; LV: left valve.

into the Indian Ocean. In contrast, glacial periods are characterized by reduced precipitation and the intensification of the winter monsoon (winds from the NE), which caused increased mechanical weathering in the source areas and led to higher dust flux rates to the Indian Ocean (Fig. 1; Kunkelova et al., 2018; Lindhorst et al., 2019).

3.3. The ostracod fauna

Core samples from Site U1467 yielded a profuse, diverse, and well-preserved ostracod fauna composed of a mixture of bathyal and shallow marine taxa over the interval spanning the past 1.2 Myr. The samples yielded an average density of 221 valves per 35 cm^3 of sample volume with a range from 39 to 920 valves per sample (or ~ 50 to 810 valves per 30 g of sediment). The ostracod assemblage consists of over 60 circumtropical and cosmopolitan ostracod genera, and twice as many species. Limited published taxonomic resources on ostracods from the Maldives and the tropical Indian Ocean calls for further taxonomic work to differentiate all the species due to the number of potentially new species found in this study. In this work, we investigate the ostracod fauna at the genus level. In Fig. 2, we show the ostracod abundance and diversity (Simpson) records compared to sediment grain size, XRF-derived lithogenic and biogenic element ratios, the HPA bottom water oxygenation index, total alkenone concentration, and the benthic $\delta^{18}O$ isotope record from Site U1467 to illustrate the relationship between the paleoceanographic proxies and the total ostracod assemblage. Overall, ostracods increase in abundance through time from the base of the record to the present, however, this trend is not constant, but interrupted by marked drops at ~0.9 Myr, 0.56 Myr, 0.4 Myr and 0.13 Myr. High abundance peaks are observed during marine isotope stages (MIS) 30, 20, 12, 8, 6, and 2. Ostracod diversity is lowest and more variable at the base of the record and is consistently high from 600 kyr to the present, except at two short intervals during MIS 14 and MIS 2. The most common ostracod genera are (their mean relative frequency in parenthesis): *Bradleya* (14%), *Cytherella* (11%), *Cytheropteron* (10%), *Krithe* (8%) and *Argilloecia* (6%). Other common genera are *Parakrithe* (5%), *Xestoleberis* (4%), *Polycope* (3%), *Agrenocythere* (3%), *Loxoconcha* (3%), *Pseudocythere* (3%), *Palmoconcha* (2%), *Saida* (2%), *Stigmatocythere* (2%) and *Cardobairdia* (2%). Bairdiid genera *Paranesidea, Neonesidea*, *Triebelina* and *Pterobairdia* are also common in some samples and are discussed as a group. Bairdiids have a combined relative frequency of 5%. Representative species of the key genera at Site U1467 are illustrated in Fig. 3.

The predominant genus, *Bradleya*, is represented mainly by *Bradleya* sp. A (most common) and *Bradleya thomasi* (Steineck and Yozzo, 1988). *Bradleya* is very common throughout the record but is generally more abundant in samples with coarser mean grain size (>50 μm) from 1.2 to 0.9 Myr and during most glacial periods, especially MIS 34, 30, 22, MIS 8 and 2 (Fig. 4). These intervals are characterized by heavier $\delta^{18}O$ values, and lower HPA values and lower alkenone concentrations, which are interpreted as more oxygenated and colder bottom water conditions, and low sea surface productivity, respectively. *Bradleya* is a marine epifaunal genus that is commonly associated with deep, oligotrophic and well oxygenated environments, and water temperatures ranging from 3.2 to 10 °C (Didié and Bauch, 2000; Mazzini, 2004; Alvarez Zarikian, 2015). In the Indo-Pacific region, some species of *Bradleya* are known from relatively shallow water depths, i.e., *Bradleya andamanae* from the outer continental shelf to the bathyal zone in the northern Indian Ocean (Benson, 1972; Whatley and Zhao, 1988; Nishath et al., 2017) and *B. albatrossia* from bathyal depths in the South China Sea [Benson, 1972; Zhao and Wang, 1990; Zhao and Zheng, 1996), thus extending the depth range for the genus from >3000 m to ~100 m.

Cytherella is the second most common genus overall. It is predominant during the MPT and before the MBE when it averages 17% and reaches up to 41% of the assemblage. Stratigraphic intervals with highest *Cytherella* abundances are centered at MIS 31, 29, 24, 21, 18, 14, and 5 (Fig. 4). These periods generally coincide with intervals of lower overall ostracod abundances, high HPA values (low bottom oxygenation), and in most cases finer grain size (except in MIS 14 and 18 when they are coeval with increases in sediment grain size). *Cytherella* decreases significantly during MIS 13 and remain scarce during most of the late Pleistocene, except during MIS 5 and MIS 1 when it shows a moderate rebound. *Cytherella* is widespread, common, and diverse along continental margins, and it inhabits bathyal and abyssal environments (Whatley and Coles, 1987; Corbari et al., 2005; Bergué et al., 2007; Brandão, 2008a). Cytherellids are filter-feeding, brooding ostracods with a sedentary lifestyle (Swanson et al., 2005) and are known to cope with low dissolved oxygen levels (Corbari et al., 2005). Previous studies have shown a link between high dominance of *Cytherella* in low diversity fossil ostracod assemblages and sediments deposited under low dissolved oxygen conditions (Whatley, 1991; Whatley et al., 2003; Corbari et al., 2005; Swanson et al., 2005). These authors argued that cytherellids can cope with low dissolved oxygen concentrations because they possess numerous, large respiratory plates that they use to enhance water circulation inside the carapace, and because they possess thick valves that can close hermetically thanks to powerful adductor muscles. However, the relationship between low oxygenated environments and high abundances of fossil cytherellids has been challenged in recent years (Brandão and Horne, 2009) because of a lack of comprehensive modern ecological data and experimental studies to support those environmental interpretations. Notwithstanding, our results show good correspondence between stratigraphic intervals of high *Cytherella* abundances and low bottom water ventilation inferred by the HPA record (Fig. 4) and results from a recent study of pteropod proxies from Site U1467 (Sreevidya et al., 2019) that concluded that intervals of intense water stratification, a sign of poor ventilation or weakened circulation, were prevalent before MIS 14.

Cytheropteron is the third most abundant and the most diverse genus at the site. It is continuously present throughout the record but increases in absolute and relative abundances during glacial to interglacial transitions and it reaches nearly 40% of the assemblage during the last deglaciation (end of MIS 2). Increases in *Cytheropteron* show good correspondence with high Fe/K values (Fig. 4), which are interpreted as periods of dry conditions and higher dust input into the northern Indian Ocean (Kunkelova et al., 2018), and during climate transitions. At least six species of *Cytheropteron* were recognized *C. hadriaticum*, *C. haoae, C. alabarda, C. bispinea, C. pulcinella,* and *C. excisum,* among others. These species are known across the northern Indian Ocean from the Red Sea to the South China Sea living at water depths ranging from ~50 up to 1000 m (Bonaduce et al., 1976; Whatley and Zhao, 1987; Zhao et al., 2000). *Cytheropteron* is a marine epifaunal and opportunistic genus with worldwide distribution and includes shallow and deep-water species (Zhao et al., 2000; Stepanova et al., 2004; Yasuhara and Okahashi, 2014; Yasuhara et al., 2009, 2014; Yamada et al., 2014; Jöst et al., 2018). They are fast-moving ostracods able to crawl and swim just above the seafloor where they are known to prey or scavenge for food, e.g., polychaetes (Hartmann, 1975). Previous studies on late Quaternary ostracods have linked high *Cytheropteron* abundances to well-oxygenated conditions

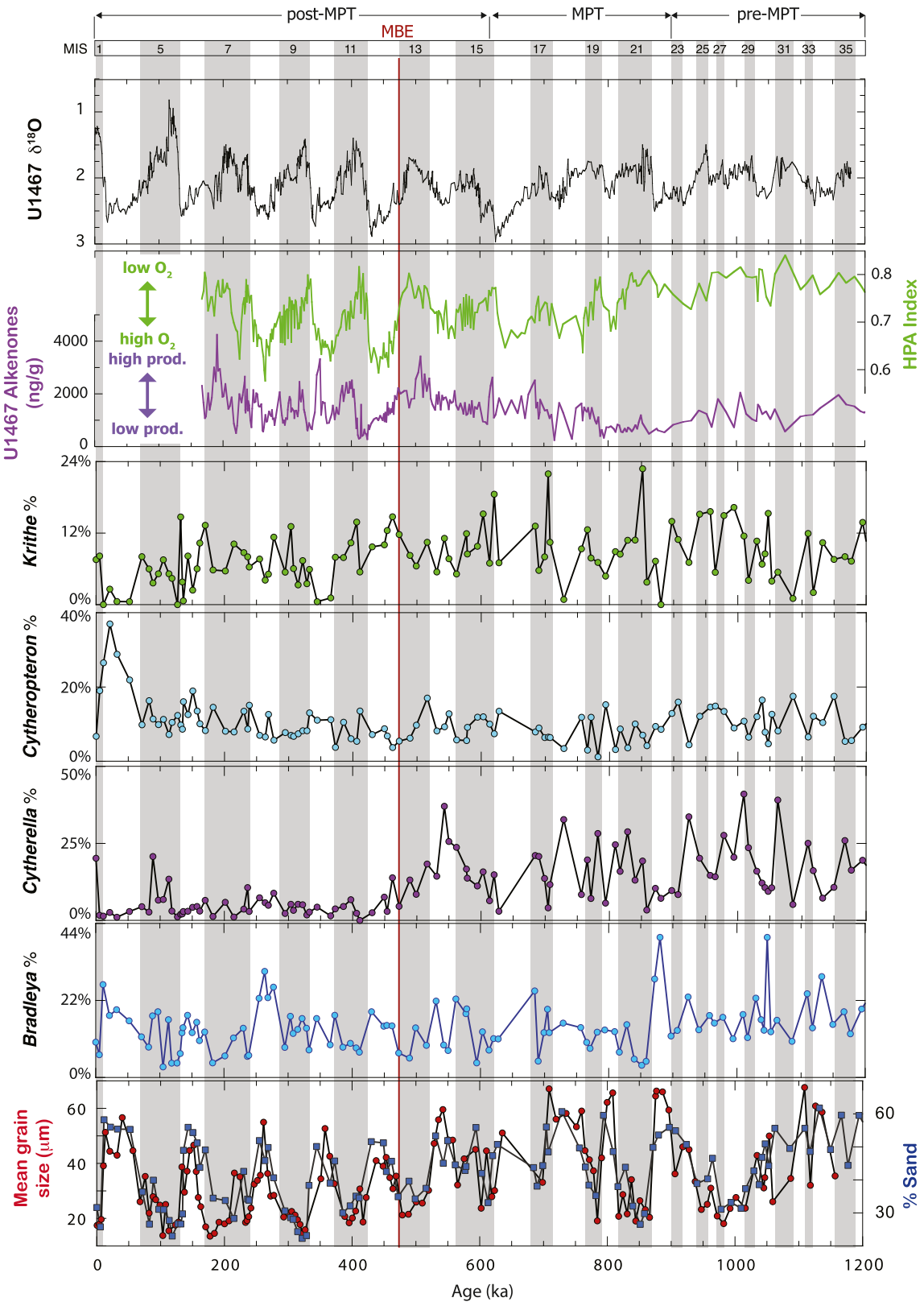

Fig. 4. Records of the predominant ostracod genera *Bradleya, Cytherella, Cytheropteron* and *Krithe* at Site U1467 compared to the environmental proxies. Bottom: the bulk sediment mean grain size (μm, dark red circles) and the proportion (%) of sand (>63 μm) in the ostracod samples (blue squares). Top half: total alkenone concentration (ng/g; purple line) from Alonso-Garcia et al. (2019) and this study; the higher plant n-alcohols/n-alkanes (HPA) ventilation index (green line). No biomarker data is available for MIS 1–6. The HPA index represents organic matter preservation, and therefore oxygenation, on the seafloor, and the total alkenone concentration sea surface primary productivity (Alonso-Garcia et al., 2019). The Site U1467 benthic $\delta^{18}O$ record from Stainbank et al. (2020). Interglacial Marine Isotope Stages (MIS) are highlighted by gray bars. The Mid-Brunhes event (MBE) is marked by the vertical dark red line at ~480 kyr. The MBE marks the increase in amplitude of glacial-interglacial cycles at the transition between MIS 13 and 12. (For interpretation of the references to colour in this figure legend, the reader is referred to the web version of this article.)

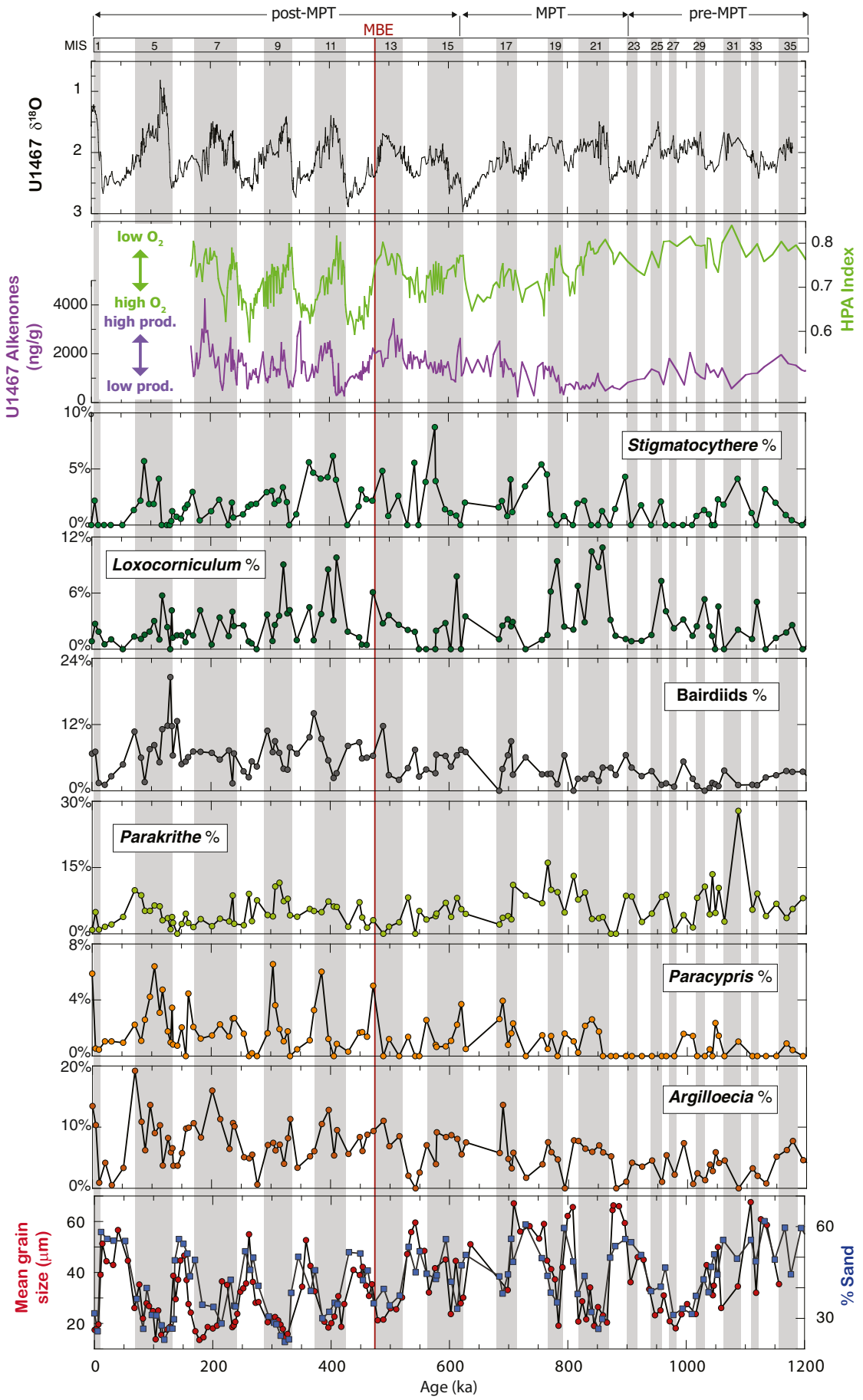

(caption on next page)

Fig. 5. Records of ostracod genera with a predominant interglacial distribution (*Argilloecia, Paracypris, Parakrithe,* bairdiids, *Loxoconcha* and *Stigmatocythere*) compared to environmental proxies. Top half: total alkenone concentration (ng/g; purple line) from Alonso-Garcia et al. (2019) and this study; the higher plant n-alcohols/n-alkanes (HPA) ventilation index (green line). No biomarker data is available for MIS 1–6. The HPA index represents organic matter preservation, and therefore oxygenation, on the seafloor, and the total alkenone concentration sea surface primary productivity (Alonso-Garcia et al., 2019). The Site U1467 benthic $\delta^{18}O$ record from Stainbank et al. (2020). Interglacial Marine Isotope Stages (MIS) are highlighted by gray bars. The Mid-Brunhes event (MBE) is marked by the vertical dark red line at ~480 kyr. The MBE marks the increase in amplitude of glacial-interglacial cycles at the transition between MIS 13 and 12. (For interpretation of the references to colour in this figure legend, the reader is referred to the web version of this article.)

and climate transitions (Cronin et al., 1999; Alvarez Zarikian et al., 2009; Huang et al., 2018). Our results are consistent with this interpretation.

The fourth most copious genus is *Krithe*, which shows higher densities during interglacial periods. *Krithe* (Fig. 4) is considered to have an infaunal lifestyle (Majoran and Agrenius, 1995) and is the most common genus in the deep sea around all the world oceans. In the Indo-Pacific region, species of *Krithe* are found at water depths ranging from 480 to 4100 m (Zhao and Zheng, 1996; Zhao and Whatley, 1997; Iwatani et al., 2018). Previous works on late Quaternary deep-sea ostracods in subtropical to subpolar regions have documented *Krithe* as indicative of deep, cold and low oxygen marine conditions (Cronin et al., 1996; Yasuhara et al., 2012; Stepanova and Lyle, 2014; Huang et al., 2018). In the Maldives Inner Sea it seems to be linked to reduced bottom water ventilation based on the geochemical environmental proxies.

The remaining common ostracod genera at Site U1467 can be separated into two groups based on their stratigraphic distribution. One group consists of genera that record their highest relative abundances in samples with low mean grain size (high mud content, reduced bottom current intensity), high alkenone concentration (higher surface productivity) and high HPA values (low bottom oxygenation) that correspond to interglacial periods (Fig. 5). These include *Argilloecia*, *Paracypris, Parakrithe*, *Paradoxostoma, Pseudocythere,* and *Xestoleberis*. Most genera in this group have smooth, slender carapaces, which is considered a morphological feature indicative of an infaunal habitat (Coles et al., 1994; Majoran and Agrenius, 1995; Tanaka, 2009). *Argilloecia*, the most common genus in this group, is predominantly found in modern low-oxygen, often organic-rich seafloor sediments (Yasuhara et al., 2008) and high abundances of *Argilloecia* in core-derived records have been interpreted as an indicator of relatively warm and low oxygen bottom waters (Cronin et al., 1996; Yasuhara et al., 2008; Alvarez Zarikian et al., 2009; Angue Minto'o et al., 2015). *Xestoleberis* are marine generally phytal ostracods that live on algae in near-shore and intertidal environments (Kondo et al., 2005). Other ostracods showing a preferred interglacial distribution are neritic taxa *Loxoconcha, Loxoconchella*, *Paraquadracythere*, *Stigmatocythere*, and *Mutilus*. Species of these genera are common in muddy and organic matter rich sediments in the Red Sea, the Gulf of Aden and the Arabian Sea (Hartmann, 1964, 1974; Bonaduce et al., 1976, 1980; Bhandari, 2004; Mohammed and Keyser, 2012; Munef et al., 2012). In addition, bairdiids *Paranesidea, Neonesidea*, *Pterobairdia* and *Triebelina* also peak during interglacial periods (Fig. 5). Although some genera in the Bairdiidae family inhabit the deep sea (Brandão, 2008b), bairdiids are more typical of shallow reef environments where they are most abundant (Maddocks, 1969b, 2013, 2015; Titterton and Whatley, 1988; Howe and McKenzie, 1989; Maddocks and Wouters, 1990; Babinot and Degaugue-Michalski, 1996; Hussain et al., 2004; Jellinek, 1993; Mckenzie and Peypouquet, 1984; Whatley and Zhao, 1987).

In contrast, we observed a group of ostracod genera with significantly higher relative abundances during glacial periods when environmental proxies indicate enhanced bottom circulation and oxygenation of the bottom water (coarser mean grain size and low HPA values) (Fig. 6). The group includes *Polycope, Agrenocythere*, *Henryhowella*, *Palmoconcha, Saida* and *Bythoceratina*. The genus *Polycope*, which averages <1% during most of the early and middle Pleistocene, increases to a range of 5% to 20% of the assemblage during most glacial periods. *Polycope* is especially abundant during MIS 6 and at the MIS 12/11 transition. Polycopids are benthic ostracods capable of swimming and have wide ecological adaptions, living in many different marine environments from tropical to high latitudes seas, from shallow marine beaches and continental shelves, to bathyal and abyssal depths, and they are very abundant in the Arctic Ocean (e.g., Cronin et al., 1995; Mazzini, 2004; Yasuhara et al., 2008; Karanovic and Tanaka, 2013; Tanaka et al., 2014; Karanovic and Brandão, 2016; Gemery et al., 2017). *Agrenocythere* is known as an epibenthic, psychrospheric genus commonly found in the deep sea (Benson, 1972). Two species are recognized in the Maldives Inner Sea record: *A. spinosa* (Benson, 1972) and *Agrenocythere* sp. (Fig. 3). In the Indian Ocean, *Agrenocythere spinosa* has been documented living at water depths ranging from 400 to 1600 m (Benson, 1972). Fossil specimens of this species were found in Pliocene sediments in Indonesia that are inferred to have been deposited in an outer shelf to bathyal marine paleoenvironment (Shin et al., 2019). *Henryhowella* is an epibenthic, deep sea genus considered to prefer well-oxygenated environments (Didié and Bauch, 2002). Ecological preferences for *Bythoceratina, Saida, and Palmoconcha* are not well known.

3.4. Multivariate analyses

The NMDS results are shown in Figs. 7 and 8. Fig. 7 illustrates the relative positions of samples and ostracod genera in a two-dimensional space, allowing us to readily interpret the faunal data. Because the two axes in Fig. 7 can be rotated, the positive and negative values along an axis are not absolute, and they simply represent the two sides of an axis. Assemblages with more different ostracod faunal compositions will be further away from each other in the plot. To explore the long-term effect of a major climatic event, we assigned different colors to the samples from before (green circles) and after (purple circles) the mid-Brunhes event. Pre-MBE and post-MBE samples plot separately to the left (negative) and right (positive) sides of the horizontal axis (NMDS1), respectively. In Fig. 7, we also indicate the position of the major indicator genera plotted in Figs. 4 through 6. *Cytherella* and *Polycope*, for example, are clearly far apart on opposite sides along the NMDS1 axis, indicating that *Cytherella* is strongly associated with pre-MBE environmental conditions and *Polycope* with the post-MBE environmental conditions in the Maldives Inner Sea. On the other hand, the glacial-interglacial climatic influence is revealed along the vertical axis (NMDS2), showing the interglacial predominant taxa *Argilloecia*, *Loxoconchella, Loxoconcha*, *Paraquadracythere*, *Paracyris*, *Parakrithe*, *Stigmatocythere*, *Cardobairdia* and bairdiids grouped in the lower (negative) side of the NMDS2 axis, and the glacial predominant taxa *Bradleya*, *Cytheropteron*, *Polycope, Agrenocythere*, *Saida*, *Palmoconcha* and *Bythoceratina* in the upper (positive) side of the axis. In Fig. 8A, the NMDS1 and NMDS2 results are plotted in relation to the Site U1467 benthic $\delta^{18}O$ record of Site U1467 (Stainbank et al., 2020). The NMDS1 generally shows an inverse correlation with the climate record before the MBE and a positive correlation with glacial/interglacial cyclicity in the late Pleistocene. The NMDS2, by contrast, shows a robust positive correlation with the climate record along the entire record.

Q-mode k-means clustering divided the samples into three clusters (Fig. 8B). Based on their tendency, Clusters 1, 2, and 3 are considered to reflect pre-MBE (before ~480 ka), interglacial, and glacial periods, respectively. Indicator Value results suggest the indicator genera for each cluster: Cluster 1 (pre-MBE): *Cytherella*; Cluster 2 (Interglacials): *Argilloecia*, bairdiids, *Krithe*, *Loxoconchella*, *Loxoconcha*, *Paraquadracythere*, *Paracypris*, *Parakrithe*, *Pseudocythere*, *Stigmatocythere*, and *Cardobairdia*. Cluster 3 (glacials): *Bradleya*, *Bythoceratina*, *Cytheropteron*,

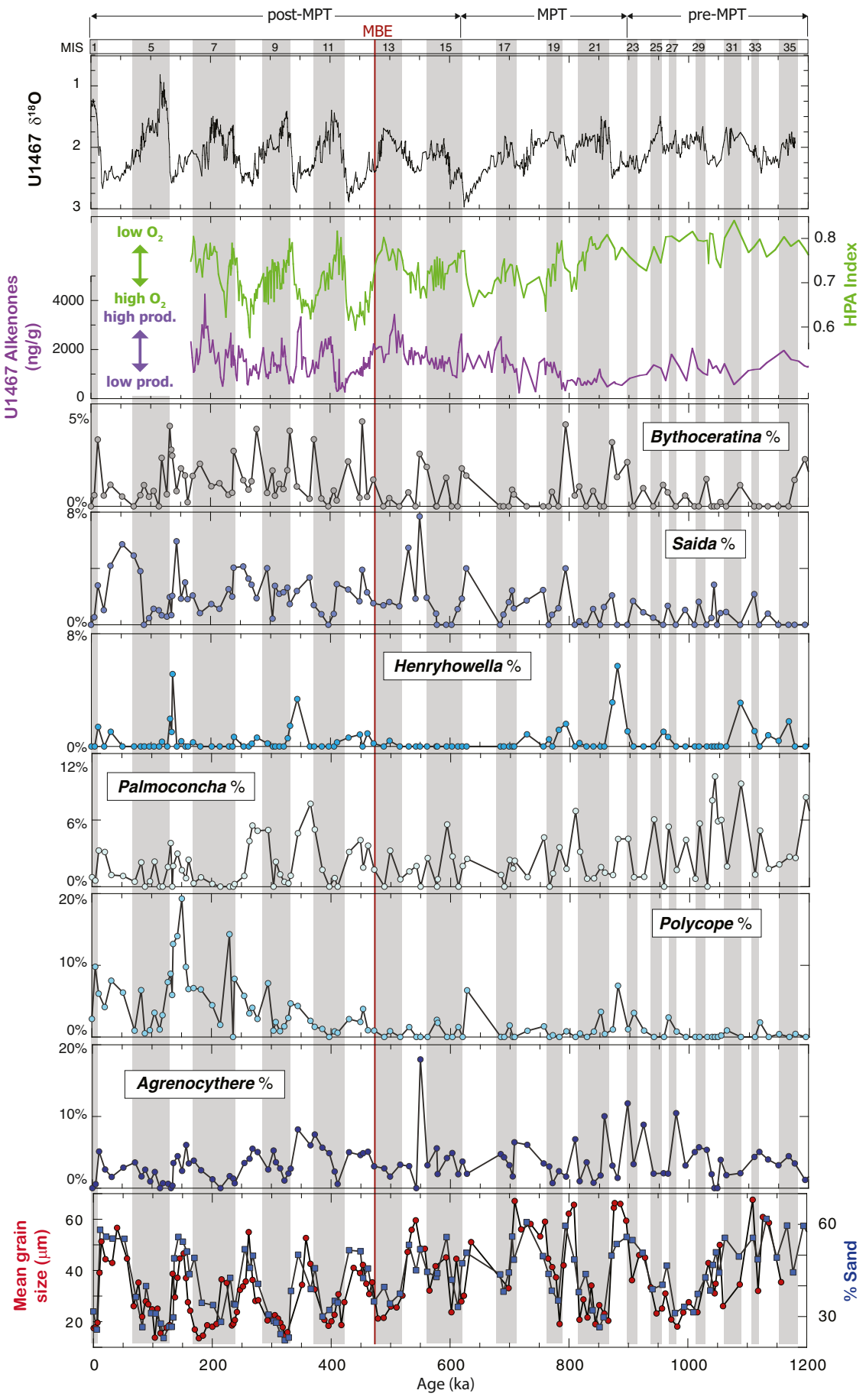

(caption on next page)

Fig. 6. Records of ostracod genera with a predominant distribution during glacial periods (*Agrenocythere, Polycope, Palmoconcha, Henryhowella, Saida* and *Bythoceratina*) compared to environmental proxies. Top half: total alkenone concentration (ng/g; purple line) from Alonso-Garcia et al. (2019) and this study; the higher plant n-alcohols/n-alkanes (HPA) ventilation index (green line). No biomarker data is available for MIS 1–6. The HPA index represents organic matter preservation, and therefore oxygenation, on the seafloor, and the total alkenone concentration sea surface primary productivity (Alonso-Garcia et al., 2019). The Site U1467 benthic $\delta^{18}O$ record from Stainbank et al. (2020). Interglacial Marine Isotope Stages (MIS) are highlighted by gray bars. The Mid-Brunhes event (MBE) is marked by the vertical dark red line at ~480 kyr. The MBE marks the increase in amplitude of glacial-interglacial cycles at the transition between MIS 13 and 12. (For interpretation of the references to colour in this figure legend, the reader is referred to the web version of this article.)

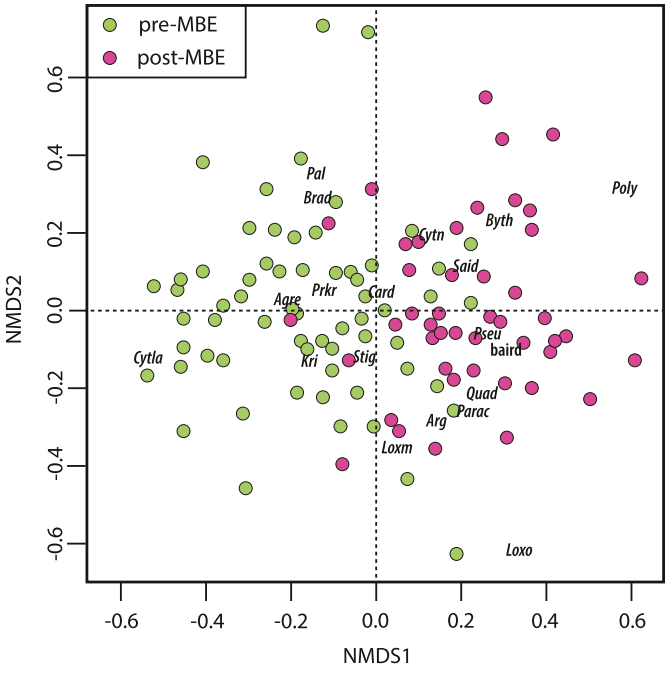

Fig. 7. Non-metric Multidimensional Scaling (NMDS) plot of the ostracod data. Solid circles represent pre-MBE (green) and post-MBE (purple) samples. Major indicator genera are indicated: *Cytherella* (*Cytla)* is strongly associated with the pre-MBE samples as shown on the left of the horizontal axis (NMDS1). Across the vertical axis (NMDS2), predominant interglacial taxa *Argilloecia* (Argi), *Bairdiids* (Bai), *Cardobairdia* (Car), *Krithe* (Kri), *Loxoconchella* (Loxa), *Loxoconcha* (Lox), *Paracypris* (Parac), *Parakrithe* (Parak), *Paraquadracythere* (Paraq), *Pseudocythere* (Pse) and *Stigmatocythere* (Sti) plot on bottom half, and predominant glacial taxa *Bradleya* (Bra), *Agrenocythere* (Agre), *Cytheropteron* (Cytn), *Bythoceratina* (Byt), *Palmoconcha* (Pal), *Polycope* (Pol), *Saida* (Sai) plot on the top half. (For interpretation of the references to colour in this figure legend, the reader is referred to the web version of this article.)

Polycope, *Saida*, *Palmoconcha*, and *Agrenocythere*. Although some of the listed indicator genera are not statistically significant based on their *p*-value (i.e., *Agrenocythere, Palmoconcha* in Fig. 8B), we consider them important assemblage components based on their stratigraphic distribution and variability with relation to climate variability.

3.5. Paleoenvironmental interpretation and history of the OMZ in the Maldives Inner Sea

The northern Indian Ocean is home to one of the major OMZs in the world, which seasonally expands southward with the intensification of the summer monsoon, which causes the input of organic matter and reduces ventilation (Lachkar et al., 2018). Bottom water ventilation in the Maldives Inner Sea is linked to the regional extension of the OMZ. Variations in the monsoon prevailing winds and precipitation patterns in the northern Indian Ocean control primary surface productivity in the Inner Sea (Alonso-Garcia et al., 2019) and influence the carbon flux to the sea bottom and oxygenation of its bottom water, affecting benthic organisms (Gupta et al., 2006).

Site U1467 lies in an oligotrophic region of the Indian Ocean making it suitable to study changes in surface productivity and OMZ expansion due to monsoonal oscillations (Sarkar and Gupta, 2009, 2014). The new integrated micropaleontological (ostracods), sedimentological, and geochemical data derived from Site U1467 provide new information useful for assessing the paleoceanographic history of the Maldives Inner Sea and the OMZ in the northern Indian Ocean over the past 1.2 Myr. In the present day, the Maldives Inner Sea has a strong temperature stratification with a sharp thermocline at a water depth of 80–90 m. Temperatures vary from ~28.5 °C in the sea surface mixed layer to ~12 °C below the thermocline, and at 500 mbsl (Reolid et al., 2017; Betzler et al., 2017a). Dissolved oxygen concentrations range from ~4 ml/l in the upper mixed layer to 1.12–1.34 ml/l below the thermocline, and to a minimum of ~0.9 ml/l at ~500 mbsl. Salinity varies from ~35.8 to 35.3 psu above and below the thermocline, respectively (Reolid et al., 2017).

Paleoclimate records from the northern Indian Ocean suggest that SAM intensity is sensitive to orbital forcing and revealed changes in sea-surface temperature (SST), wind patterns, productivity, and OMZ extension during the past climatic cycles (Bolton et al., 2013; Caley et al., 2011; Clemens and Prell, 2003; Kunkelova et al., 2018; Alonso-Garcia et al., 2019; Lindhorst et al., 2019). The Maldives monsoonal record of the past 2 Myr, interpreted from the variability of lithogenic components in cores from Site U1467 (Kunkelova et al., 2018; Lindhorst et al., 2019), shows the intensification of the SAM during MIS 12 because of increasingly drier climatic conditions in southern Asia and stronger winter monsoon winds, which led to progressively higher eolian induced dust input into the Inner Sea during glacials. Contrastingly, stronger summer monsoon (southwesterly winds) generated wetter conditions and increased fluvial input into the northern Indian Ocean during interglacial periods. These interpretations are supported by biomarker proxies for sea surface temperature (SST), precipitation, and primary productivity (Alonso-Garcia et al., 2019) that indicate generally drier conditions in glacial periods and increased precipitation and warmer SST during interglacials, although such conditions were not always exclusive of those intervals.

Non-metric multidimensional scaling of the Site U1467 ostracod data (Fig. 8) shows remarkable correspondence between both the NMDS1 and NMDS2 and the Site U1467 benthic $\delta^{18}O$ record, demonstrating that SAM intensification and bottom water ventilation variability in the Inner Sea had a direct effect on ostracod assemblage composition, and underscoring the ostracods sensitivity to past climate and oceanographic variability. The results show a significant change in ostracod assemblage composition at the MBE related to the increase in the amplitude of glacial-interglacial cycles, which deeply affected the monsoon system and thereby the Maldives Inner Sea. Furthermore, ostracods exhibit distinctly different assemblages across glacial-interglacial cycles, particularly after the MBE, and these changes convincingly correspond to the contractions and expansions of the OMZ.

The ostracod record suggests prevailing low bottom water oxygenation and intense OMZ in the Inner Sea between ~1200 ka and ~ 870 ka (pre MPT) as interpreted by the relatively low ostracod abundances and a predominance of *Cytherella* and *Parakrithe*. A recent study using pteropod abundances and preservation changes at Site U1467 for reconstructing the OMZ strength, past oceanic carbonate saturation and dissolution events in the Maldives supports a period of intense water column stratification and carbonate dissolution between ~1200 ka and ~ 850 ka (Sreevidya et al., 2019). During the MBE, a major change takes place in the ostracod assemblage composition, resulting in the

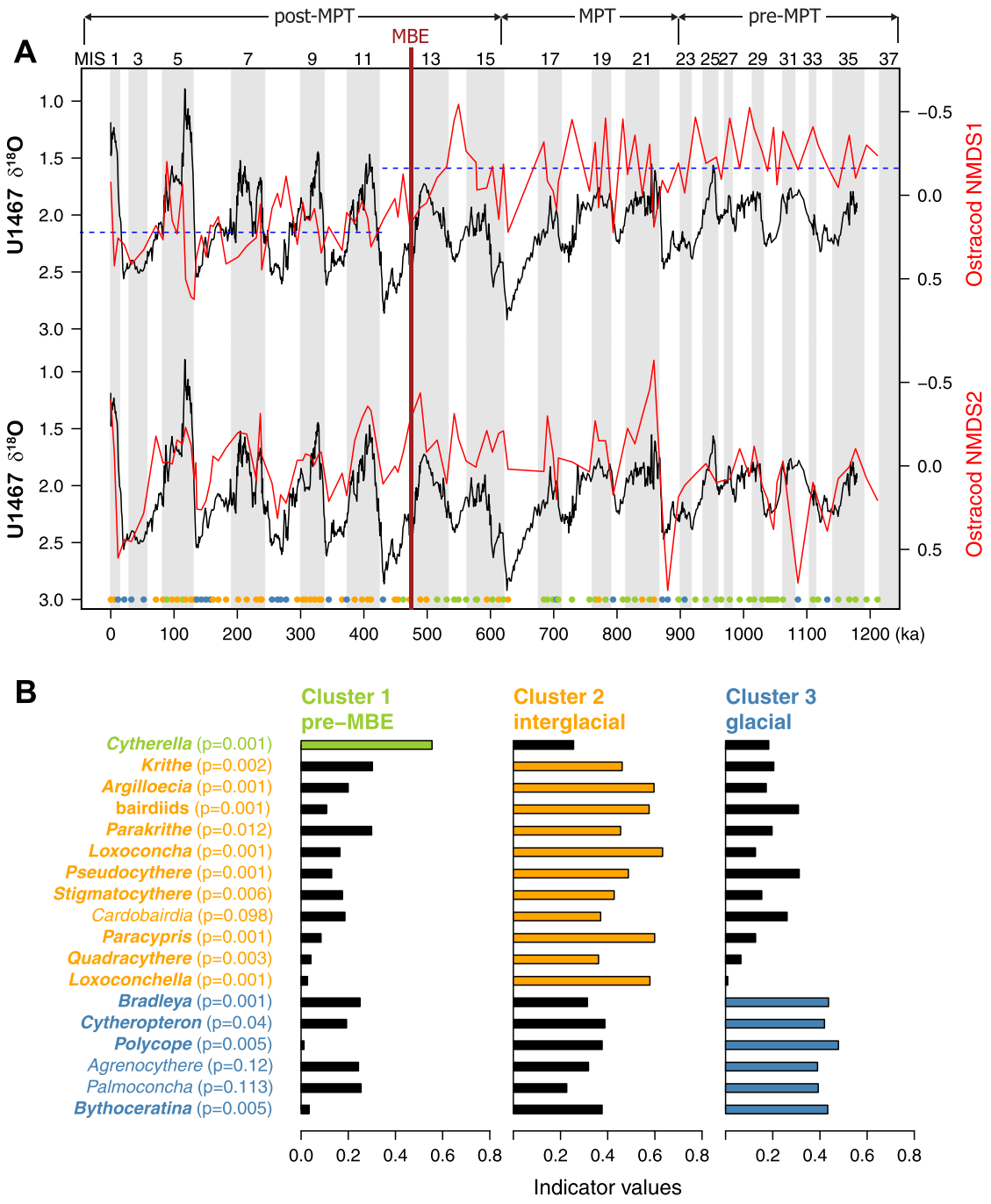

Fig. 8. (**A**) The ostracods NMDS1 and NMDS2 plotted against the U1467 benthic $\delta^{18}O$ record (Stainbank et al., 2020). Note the excellent agreement between the NMDS2 curve and the climate record. The blue dotted lines indicate the average values of NMDS1 in pre-MBE and post-MBE periods. Interglacial marine isotopic stages are annotated on the top and indicated on the background by gray vertical lines. MPT = Mid-Pleistocene Transition; MBE = Mid-Brunhes Event. Solid circles across the base of the figure represent the samples of this study, and their colors correspond to the clusters in the bottom panel. (**B**) Indicator values of major genera for Clusters 1 (green; pre-MBE), 2 (orange; Interglacial), and 3 (blue; glacial). The genera in bold are significant indicators with a *p*-value <0.05 in the permutation test. Ostracod genera names are colored according to the clusters the genera have the highest indicator values for. For example, the indicator values of *Argilloecia* are 0.19, 0.59, 0.17 for Clusters 1, 2, and 3, respectively. *Argilloecia* has the maximum indicator value in Cluster 2, so it is considered an indicator genus for this cluster. Based on their tendency, Clusters 1, 2, and 3 are considered to reflect the ostracod assemblage before the Mid-Brunhes Event (MBE), and during interglacial and glacial periods, respectively. (For interpretation of the references to colour in this figure legend, the reader is referred to the web version of this article.)

development of two distinct assemblages that are driven by glacial and interglacial oceanographic conditions. During interglacials, associated with finer sediment grain size, poor seafloor oxygenation (high HPA values) and generally high primary productivity (high alkenone concentrations), an assemblage of mostly infaunal/interstitial ostracods (e.g., *Argilloecia, Paracypris,* and *Parakrithe*) point to an intensification of the OMZ and reduced ventilation in the Maldives Inner Sea. Pteropod data from Site U1467 (Sreevidya et al., 2019) and benthic foraminifera data from ODP Site 716A (Sarkar and Gupta, 2014) also indicate intensification/expansion of the OMZ during interglacial stages due to prominent stratification events or high organic flux to the seafloor. Glacial stages, by contrast, are distinguished by the predominance of

ostracods that suggest well-oxygenated and colder bottom water (e.g., *Bradleya, Henryhowella,* and *Agrenocythere* among others). This is also supported by Inner Sea thermocline reconstructions (Stainbank et al., 2021) that show warmer surface waters, highly stratified water column and a stronger thermocline at the MIS11c climate maximum, compared to less stratification and weak thermocline during both the LGM and MIS12 climate maxima. Differently from earlier glacial periods, MIS 2, 6, and 8 exhibit significant abundance peaks in *Polycope* and *Cytheropteron*. A previous multiproxy study in the Maldives Inner Sea revealed increased surface productivity and related organic carbon fluxes during MIS 2 and 6 because of the combined effects of wind-induced mixing of surface waters and dust fertilization during cold phases (Bunzel et al., 2017). Peaks in *Polycope* and *Cytheropteron,* opportunistic genera that commonly dominate climatic transitions in core derived sediments (Alvarez Zarikian et al., 2009; Huang et al., 2019) could be related to increased productivity in well-oxygenated conditions. Pteropod abundance and preservation data from Site U1467 (Sreevidya et al., 2019) suggest enhanced water column mixing and ventilation during glacials, and glacial to interglacial periods, except during MIS 14 when intense stratification, and poor ventilation or weakened circulation was inferred. Good aragonite preservation during glacial periods has been attributed to very low atmospheric CO_2, enhanced ventilation and strengthened influx of Subantarctic Mode and Antarctic Intermediate Waters (SAMW-AAIW) and weakening of the OMZ (Böning and Bard, 2009; Sreevidya et al., 2019). The advection of well oxygenated southern sourced intermediate water (Reichart et al., 1997; Jung et al., 2009) may explain the increase of typically deep-sea ostracods *Bradleya, Henryhowella,* and *Agrenocythere* in the Maldives Inner Sea during glacial periods.

4. Conclusions

The Maldives Inner Sea sediment drifts sampled by IODP Site U1467 provide an archive of a well preserved and abundant microfossil record spanning the Pleistocene era and that is suitable for investigating the South Asian Monsoon system and its effects on primary productivity, ocean currents, and bottom ventilation. In the long-term, non-metric multidimensional scaling (NMDS) of the ostracod data revealed a major faunal turnover around 480 ka (MIS 13/12). The middle Pleistocene ostracod assemblage was characterized by the predominance of *Cytherella*, which suggests reduced bottom water ventilation in the Maldives Inner Sea and therefore an expanded OMZ in the northern Indian Ocean. Organic geochemical data indicate low sea surface productivity and warm surface water temperatures and sluggish bottom current (poor ventilation) prevailed during this period. Cooling climate stages of the mid-Pleistocene were marked by increases in the abundance of high oxygen ostracod indicators (e.g., *Bradleya, Agrenocythere*). The NMDS results also revealed a remarkable synchroneity between glacial/interglacial climate cycles and ostracod assemblage variability. Glacial stages are predominantly characterized by ostracods indicators of well-oxygenated bottom waters, and possibly enhanced intermediate water flow driven by the intensification of the winter monsoon and northward extension of the influence of Glacial Antarctic Intermediate Water. Interglacial stages, in contrast, are characterized by ostracods that indicate low-oxygen and sluggish bottom circulation pointing to high sea surface productivity and organic flux to the seafloor with periods of strong water column stratification events due to the intensification of the summer monsoon. The alternation between glacial and interglacial ostracod assemblages shows good correspondence with the organic biomarker proxies indicative of changes in sea surface productivity (total alkenone concentration) and bottom water ventilation (HPA index). The excellent correlation between the climate and oceanographic proxies and the ostracod data clearly shows the response of benthic organisms to the glacial-interglacial changes, and highlights the suitability of ostracods, even at the genus level, for paleoenvironmental and paleoceanographic reconstructions.

Author contributions

CAAZ was the project manager of IODP Expedition 359, designed this study, led the sample analysis, ostracod characterization and interpretation, led the manuscript preparation, and contributed to the XRF core scanning. CN processed the sediment samples, contributed to the ostracod characterization, statistical analyses, and the XRF core scanning. MAG contributed to shipboard handling, biostratigraphy of the cores, XRF core scanning, and performed the analysis and quantification of the lipid biomarkers. TR contributed to the analysis and quantification of the lipid biomarkers. HHMH and MY contributed to the statistical analysis, ostracod identification and interpretation. DK contributed to shipboard handling, biostratigraphy of the cores, XRF core scanning and XRF data interpretation, and the stable isotope record. TK contributed to XRF data analysis and interpretation. SL performed the grain size analysis. CB served as Co-Chief scientist of Expedition 359 and contributed to grain size analysis. All authors contributed to the discussion, interpretation and writing of the manuscript.

Author statement

I certify that all authors have seen and approved the final version of the manuscript being submitted. This manuscript is the authors' original work, hasn't received prior publication and isn't under consideration for publication elsewhere. All funding sources have been disclosed in the manuscript.

Declaration of Competing Interest

The authors declare that they have no known competing interests or personal relationships that could have appeared to influence the work reported in this paper.

Acknowledgments

Expedition 359 was funded by the US National Science Foundation (NSF); the European Consortium for Ocean Research Drilling (ECORD); the Ministry of Education, Culture, Sports, Science and Technology, Japan (MEXT); the Ministry of Science and Technology (People's Republic of China); the Korea Institute of Geoscience and Mineral Resources; the Australian Research Council and the New Zealand Institute for Geological and Nuclear Sciences; and the Ministry of Earth Sciences (India). CAAZ acknowledges financial support from the U.S. Science Support Program at Columbia University under post-expedition award OCE14–50528 and NSF award no. OCE-1326927. MAG and TR would like to acknowledge funding from FCT (CCMAR UID/Multi/04326/2019 and WarmWorld project (PTDC/CTA-GEO/29897/2017). MY acknowledges funding from the Research Grants Council of the Hong Kong Special Administrative Region, China (project code: HKU 17302518), the Seed Funding Programme for Basic Research of the University of Hong Kong (project code: 202011159122), the Small Equipment Grant of the University of Hong Kong, the Seed Funding of the HKU-TCL Joint Research Centre for Artificial Intelligence, SKLMP Seed Collaborative Research Fund of City University of Hong Kong (project code: SKLMP/SCRF/0031), and the Faculty of Science RAE Improvement Fund of the University of Hong Kong. This research used samples and data provided by the International Ocean Discovery Program (IODP). This study would not have been possible without the dedicated effort of the drilling crew, ship's crew, and scientific staff of the drillship JOIDES Resolution during IODP Expedition 359. The Ministry of Fisheries and Agriculture of the Republic of the Maldives is thanked for granting the research permit. Thomas Stephens is thanked for assistance during the SEM imaging. Gene Hunt for helping with ostracod taxonomy. We thank Simone N. Brandão and an anonymous reviewer for their thoughtful comments and suggestions for improving this manuscript.

References

Ahn, S., Khider, D., Lisiecki, L.E., Lawrence, C.E., 2017. A probabilistic Pliocene–Pleistocene stack of benthic $\delta^{18}O$ using a profile hidden Markov model. Dyn. Stat. Clim. Syst. 2, 1–16. https://doi.org/10.1093/climsys/dzx002.

Alonso-Garcia, M., Rodrigues, T., Abrantes, F., Padilha, M., Alvarez-Zarikian, C.A., Kunkelova, T., Wright, J.D., Betzler, C., 2019. Sea-surface temperature, productivity and hydrological changes in the Northern Indian Ocean (Maldives) during the interval ~575-175 ka (MIS 14 to 7). Palaeogeogr. Palaeoclimatol. Palaeoecol. Volume 536, 109376. ISSN 0031-0182. https://doi.org/10.1016/j.palaeo.2019.109376.

Alvarez Zarikian, C.A., 2015. Cenozoic bathyal and abyssal ostracods beneath the oligotrophic South Pacific Gyre (IODP Expedition 329 Sites U1367, U1368 and U1370). Palaeogeogr. Palaeoclimatol. Palaeoecol. 419, 115–142. https://doi.org/10.1016/j.palaeo.2014.07.024.

Alvarez Zarikian, C.A., Stepanova, A.Y., Grützner, J., 2009. Glacial-interglacial variability in deep sea ostracod assemblage composition at IODP Site U1314 in the subpolar North Atlantic. Mar. Geol. 258, 69–87. https://doi.org/10.1016/j.margeo.2008.11.009.

Angue Minto'o, C.M., Bassetti, M.A., Morigi, C., Ducassou, E., Toucanne, S., Jouet, G., Mulder, T., 2015. Levantine intermediate water hydrodynamic and bottom water ventilation in the northern Tyrrhenian Sea over the past 56,000 years: New insights from benthic foraminifera and ostracods. Quat. Int. 357, 295–313. ISSN 1040–6182. https://doi.org/10.1016/j.quaint.2014.11.038.

Antoine, D., André, J.-M., Morel, A., 1996. Oceanic primary production: 2. Estimation at global scale from satellite (Coastal Zone Color Scanner) chlorophyll. Glob. Biogeochem. Cycles 10, 57–69.

Aubert, O., Droxler, A.W., 1992. General Cenozoic evolution of the Maldives carbonate system (equatorial Indian Ocean). Bull. Centres Rech. Explor. Prod. Elf-Aquitaine 16 (1), 113–136.

Babinot, J., Degaugue-Michalski, F., 1996. Lagoonal to reefal Ostracod assemblages from Holocene and recent deposits, Chesterfield Islands and Northern New Caledonia (Southwestern Pacific). Micropaleontology 42, 351–362. https://doi.org/10.2307/1485957.

Babinot, J.-F., Kouyoumontzakis, G., 1995. In: Geobios, M.S. (Ed.), Associations d'ostracodes d'un environment récifal envasé: le Lagon de L'Ile de Mayotte (Archipel des Comores, Océan Indien Occidental), vol. 18, pp. 17–38.

Backman, J., and Lyle, M., 2013. Data report: calibration of XRF-estimated CaCO3 along the Site U1338 splice. In Pälike, H., Lyle, M., Nishi, H., Raffi, I., Gamage, K., Klaus, A., and the Expedition 320/ 321 Scientists, Proc. IODP, 320/321: Tokyo (Integrated Ocean Drilling Program Management International, Inc.). doi:10.2204/iodp.proc.320321.205.2013.

Benson, R.H., 1972. The *Bradleya* problem, with description of two new psychrospheric Ostracode genera, *Agrenocythere* and *Poseidonamicus* (Ostracoda: Crustacea), Smithson. Contrib. to Paleobiol. 12, 1–138. https://doi.org/10.5479/si.00810266.12.1.

Benson, R.H., 1974. Preliminary Report on the Ostracods from Leg 24. Initial Reports of the Deep Sea Drilling Project, vol. 24. U.S. Government Printing Office, Washington D.C., pp. 1037–1043 (26).

Bergué, C.T., Coimbra, J.C., Cronin, T.M., 2007. Cytherellid species (Ostracoda) and their significance to the late Quaternary events in the Santos Basin, Brazil. Senckenberg. Marit. 37 (1), 5–12.

Betzler, C., Lüdmann, L., Hübscher, C., Fürstenauet, J., 2013. Current and sea-level signals in periplatform ooze (Neogene, Maldives, Indian Ocean). Sediment. Geol. 290, 126–137. https://doi.org/10.1016/j.sedgeo.2013.03.011.

Betzler, C., Lindhorst, S., Lüdmann, T., Weiss, B., Wunsch, M., Braga, J.C., 2015. The leaking bucket of a Maldives atoll: Implications for the understanding of carbonate platform drowning. Mar. Geol. 366, 16–33.

Betzler, C., Eberli, G.P., Kroon, D., Wright, J.D., Swart, P.K., Nagender Nath, B., Alvarez-Zarikian, C.A., Alonso-García, M., Bialik, O.M., Blättler, C.L., Adam Guo, J., Haffen, S., Horozal, S., Inoue, M., Jovane, L., Lanci, L., Laya, J.C., Mee, Ling Hui, Lüdmann, T., Nakakuni, M., Niino, K., Petruny, L.M., Pratiwi, S.D., Reijmer, J.J.G., Reolid, J., Slagle, A.L., Sloss, C.R., Su, X., Yao, Z., Young, J.R., 2016. The abrupt onset of the modern South Asian Monsoon winds. Sci. Rep. 07 (2016), 6. https://doi.org/10.1038/srep29838.

Betzler, C., Eberli, G.P., Alvarez Zarikian, C.A., the Expedition 359 Scientists, 2017a. Maldives monsoon and sea level. In: Proceedings of the International Ocean Discovery Program, 359: College Station, TX (International Ocean Discovery Program). https://doi.org/10.14379/iodp.proc.359.2017.

Betzler, C., Eberli, G.P., Alvarez Zarikian, C.A., Alonso-García, M., Bialik, O.M., Blättler, C.L., Guo, J.A., Haffen, S., Horozal, S., Inoue, M., Jovane, L., Kroon, D., Lanci, L., Laya, J.C., Mee, Ling Hui, Lüdmann, T., Nakakuni, M., Nath, B.N., Niino, K., Petruny, L.M., Pratiwi, S.D., Reijmer, J.J.G., Reolid, J., Slagle, A.L., Sloss, C.R., Su, X., Swart, P.K., Wright, J.D., Yao, Z., Young, J.R., 2017b. Site U1467. In: Betzler, C., Eberli, G.P., Alvarez Zarikian, C.A., the Expedition 359 Scientists (Eds.), Maldives Monsoon and Sea Level. Proceedings of the International Ocean Discovery Program, 359: College Station, TX (International Ocean Discovery Program). https://doi.org/10.14379/iodp.proc.359.105.2017.

Betzler, C., Eberli, G.P., Lüdmann, T., Reolid, J., Kroon, D., Reijmer, J.J.G., Swart, P.K., Wright, J.D., Young, J.R., Alvarez Zarikian, C.A., Alonso-García, M., Bialik, O.M., Blättler, C.L., Guo, J.A., Haffen, S., Horozal, S., Inoue, M., Jovane, L., Lanci, L., Laya, J.C., Ling Hui Mee, A., Nakakuni, M., Nath, B.N., Niino, K., Petruny, L.M., Pratiwi, S.D., Slagle, A.L., Sloss, C.R., Su, X., Yao, Z., 2018. Refinement of Miocene Sea level and monsoon events from the sedimentary archive of the Maldives (Indian Ocean). Progr. Earth Planetary Sci. 5, 5. https://doi.org/10.1186/s40645-018-0165-x.

Bhandari, A., 2004. Evolutionary trends and biostratigraphic significance of the ostracode genus *Stigmatocythere* in the Cenozoic succession of India. Paleontol. Res. 8 (3), 181–197. https://doi.org/10.2517/prpsj.8.181.

Blott, S.J., Pye, K., 2001. GRADISTAT: a grain size distribution and statistics package for the analysis of unconsolidated sediments. Earth Surf. Process. Landf. 26, 1237–1248.

Bogus, K.A., Zonneveld, K.A.F., Fischer, D., Kasten, S., Bohrmann, G., Versteegh, G.J.M., 2012. The effect of meter-scale lateral oxygen gradients at the sediment-water interface on selected organic matter-based alteration, productivity and temperature proxies. Biogeosciences 9, 1553–1570.

Bolton, C.T., Chang, L., Clemens, S.C., Kodama, K., Ikehara, M., Medina-Elizalde, M., Paterson, G.A., Roberts, A.P., Rohling, E.C., Yamamoto, Y., Zhao, X., 2013. A 500,000 year record of Indian summer monsoon dynamics recorded by eastern equatorial Indian Ocean upper water-column structure. Quat. Sci. Rev. volume 77, 167–180. ISSN 0277–3791. https://doi.org/10.1016/j.quascirev.2013.07.031.

Bonaduce, G., Masoli, M., Pugliese, N., 1976. Benthic Ostracoda from the Gulf of Aqaba, Red Sea. Publ. Stn. Zool. Napoli. 40, 372–428.

Bonaduce, G., Masoli, M., Minicheli, G., Pugliese, N., 1980. Some new benthic ostracod species from the Gulf of Aqaba Red Sea. Boll. Soc. Paleont. Italiana 19, 143–178.

Böning, P., Bard, E., 2009. Millennial/centennial-scale thermocline ventilation changes in the Indian Ocean as reflected by aragonite preservation and geochemical variations in Arabian Sea sediments. Geochim. Cosmochim. Acta 73, 6771–6788.

Borcard, D., Gillet, F., Legendre, P., 2011. Numerical Ecology with R. Springer-Verlag, New York.

Brandão, S.N., 2008a. First Record of a living Platycopida (Crustacea, Ostracoda) from Antarctic waters and a Discussion on *Cytherella serratula* (Brady, 1880), Zootaxa 1866, pp. 349–372. ISSN 1175–5334.

Brandão, S.N., 2008b. New species of Bairdioidea (Crustacea, Ostracoda) from the Southern Ocean and discussions on *Bairdoppilata simplex* (Brady, 1880), ? *Bairdoppilata labiata* (Müller, 1908) and *Bythopussella aculeata* (Müller, 1908). Zootaxa, 1866: 373–452. In: Martínez Arbizu, P., Brix, S. (Eds.), Bringing Light into Deep-sea Biodiversity. Zootaxa, 1866, pp. 1–574 (ISSN 1175-5334).

Brandão, S.N., Horne, D.J., 2009. The Platycopid Signal of oxygen depletion in the ocean: A critical evaluation of the evidence from modern ostracod biology, ecology and depth distribution. Palaeogeogr. Palaeoclimatol. Palaeoecol. 283, 126–133. https://doi.org/10.1016/j.palaeo.2009.09.007.

Bunzel, D., Schmiedl, G., Lindhorst, S., Mackensen, A., Reolid, J., Romahn, S., Betzler, C., 2017. 2017, A multi-proxy analysis of late Quaternary Ocean and climate variability for the Maldives. Inner Sea. Clim. Past 13, 1791–1813. https://doi.org/10.5194/cp-13-1791-2017.

Cacho, I., Grimalt, J.O., Sierro, F.J., Shackleton, N., Canals, M., 2000. Evidence for enhanced Mediterranean thermohaline circulation during rapid climatic coolings. Earth Planet. Sci. Lett. 183, 417–429.

Caley, T., Malaizé, B., Bassinot, F., Clemens, S., Caillon, N., Linda, R., Rebaubier, H., 2011. The monsoon imprint during the 'atypical' MIS 13 as seen through north and equatorial Indian Ocean records. Quat. Res. 76 (2), 285–293. https://doi.org/10.1016/j.yqres.2011.07.001.

Ciarapica, G., Passeri, L., 1993. An overview of the Maldivian coral reefs in Felidu and North Malé atoll (Indian Ocean): platform drowning by ecological crises. Facies 28 (1), 33–65. https://doi.org/10.1007/BF02539727.

Clemens, S.C., Prell, W.L., 2003. A 350,000 year summer-monsoon multi-proxy stack from the Owen Ridge, Northern Arabian Sea. Mar. Geol. 201 (1–3), 35–51. ISSN 0025-3227. https://doi.org/10.1016/S0025-3227(03)00207-X.

Coles, G.P., Whatley, R.C., Moguilevsky, A., 1994. The ostracod genus Krithe from the Tertiary amd Quaternary of the North Altantic. Palaentology 27 (1), 71–220.

Corbari, L., Mesmer-Dudons, N., Carbonel, P., Massabuau, J.C., 2005. *Cytherella* as a tool to reconstruct deep-sea paleo-oxygen levels: the respiratory physiology of the platycopid ostracod *Cytherella* cf. *abyssorum*. Mar. Biol. 147, 1377–1386 (2005). https://doi.org/10.1007/s00227-005-0040-3.

Cronin, T.M., Holtz Jr., T.R., Stein, R., Spielhagen, R., Fütterer, D., Wollenburg, J., 1995. Late Quaternary paleoceanography of the Eurasian Basin, Arctic Ocean. Paleoceanography 10 (2), 259–281. https://doi.org/10.1029/94PA03149.

Cronin, T.M., Raymo, M.E., Kyle, K.P., 1996. Pliocene (3.2–2.4 Ma) ostracode faunal cycles and deep ocean circulation, North Atlantic Ocean. Geology 24, 695–698. https://doi.org/10.1130/0091-7613.

Cronin, T.M., DeMartino, D.M., Dwyer, G.S., Rodriguez-Lazaro, J., 1999. Deep-sea ostracode species diversity: response to late Quaternary climate change. Mar. Micropalentol. 37, 231–249.

Dewi, K.T., 1993. Ostracoda from the Java Sea, West of Bawean Island, Indonesia. Master of Science (Hons.) Thesis. Department of Geology, University of Wollongong, 165 pages. http://ro.uow.edu.au/theses/2832.

Didié, C., Bauch, H.A., 2000. Species composition and glacial-interglacial variations in the ostracode fauna of the Northeast Atlantic during the past 200,000 years. Mar. Micropaleontol. 40, 105–129.

Didié, C., Bauch, H.A., 2002. Implications of upper Quaternary stable isotope records of marine ostracodes and benthic foraminifers for paleoecological and paleoceanographical reconstructions. In: Holmes, J.A., Chivas, A.R. (Eds.), The Ostracoda: Applications in Quaternary Research. American Geophysical Union, Washington, DC, USA, pp. 279–299.

Dufrêne, M., Legendre, P., 1997. Species assemblages and indicator species: the need for a flexible asymmetrical approach. Ecol. Monogr. 67, 345–366.

Elofson, O., 1941. Zur Kenntnis der marinen ostracoden Schwedens mit besonderer berücksichtigung des skageraks. Sonderabdruck aus Zoologiska Bidrag Fran Uppsala, Band 19, 215–515.

Fauzielly, L., Irizuki, T., Sampei, Y., 2013. Spatial distribution of recent ostracode assemblages and depositional environments in Jakarta Bay, Indonesia, with relation to environmental factors. Paleontol. Res. 16 (4), 267–281.

Folk, R.L., Ward, W.C., 1957. Brazos River bar; a study in the significance of grain size parameters. J. Sediment. Res. 27, 3–26.

Garcia, H.E., et al., 2014. World ocean atlas 2013, Volume 3: dissolved oxygen, apparent oxygen utilization, and oxygen saturation. In: Levitus, S. (Ed.), A. Mishonov Technical Ed.; NOAA Atlas NESDIS 75, 27 pp.

Gemery, Laura, Cronin, T.M., Briggs, W.M, et al., 2017. An Arctic and Subarctic ostracode database: biogeographic and paleoceanographic applications. Hydrobiologia 786, 59–95. https://doi.org/10.1007/s10750-015-2587-4.

Gopalakrishna, K., Hussain, S.M., Mahesh Bilwa, L., Ayisha, V.A., 2007. Recent benthic ostracoda from the inner shelf off the Malabar coast, Kerala, southwest coast of India. J. Palaentol. Soc. India 52 (1), 59–68.

Gopalakrishna, K., Shabi, B., Mahesh Bilwa, L., 2008. Distribution of ostracode assemblages along the nearshore and offshore areas of Malabar coast, Kerla (west coast of India). Indian J. Mar. Sci. 37 (3), 298–306.

Guernet, C., 1993. Ostracodes du plateau d'Exmouth (Océan Indien): remarques systematiques et évolution des environnements oceaniques profonds au cours du Cénozoïque. Geobios 26 (3), 345–360.

Gupta, A.K., Das, M., Bhaskar, K., 2006. South Equatorial Current (SEC) driven changes at DSDP Site 237, Central Indian Ocean, during the Plio-Pleistocene: Evidence from Benthic Foraminifera and Stable Isotopes. J. Asian Earth Sci. 28 (4–6), 276–290. ISSN 1367–9120. https://doi.org/10.1016/j.jseaes.2005.10.006.

Hartmann, G., 1964. Zur Kenntnis der Ostracoden des Roten Meeres. Kieler Meeresforschungen. Sonderheft Band XX. In: Aus dem Zoologischen Staatsinstitut und Zoologischem Museum Hamburg, Sonderdruck S, pp. 35–127.

Hartmann, G., 1974. Zur Kenntnis des Eulitorals der afrikanischen Westkfiste zwischen Angola und Kap der Guten Hoffnung und der afrikanischen Ostkiiste yon Sudafrika und Mozambique unter besonderer Beiicksichtigung der Polychaeten und Ostracoden. In: Teil 3. Die Ostracoden des Untersuchungsgebiets. - Mitt. hamb. zool, Mus. Inst, 69, pp. 229–520 (Erg. Bd).

Hartmann, G., 1975. Ostracoda. In: Gruner, H.E. (Ed.), Dr. H. G. Bronns Klassen und Ordnungen des Tierreichs. Fünfter Band: Arthropoda I. Abteilung: Crustacea 2. Buch, IV. Teil, vol. 4. Lieferung, Gustav Fischer, Jena, pp. 569–786.

Hartmann-Schröder, G., Hartmann, G., 1978. Zur Kenntnis des Eulitorals der australischen Küsten unter besonderer Berücksichtigunng der Polychaeten und Ostracoden. Mitt. Hamb. Zool. Mus. Inst. Band 75, 63–219 (ISSN 0072-9612).

Hong, Y., Yasuhara, M., Iwatani, H., Mamo, B., 2019. Baseline for ostracod-based northwestern Pacific and Indo-Pacific shallow-marine paleoenvironmental reconstructions: ecological modeling of species distributions. Biogeosciences 16, 585–604. https://doi.org/10.5194/bg-16-585-2019.

Howe, H.V., McKenzie, K.G., 1989. Recent marine Ostracoda (Crustacea) from Darwin and north-western Australia. In: Northern Territory Museum of Arts and Sciences, Darwin. Monograph Series 3. ISBN 0 7245 1821 5, ISSN 0814 0030.

Huang, H.H.M., Yasuhara, M., Iwatani, H., Alvarez Zarikian, C.A., Bassetti, M.A., Sagawa, T., 2018. Benthic biotic response to climate changes over the last 700,000 years in a deep marginal sea: impacts of deoxygenation and the Mid-Brunhes Event. Paleoceanogr. Paleoclimatol. 33 (7), 766–777. https://doi.org/10.1029/2018PA003343.

Huang, H.H.M., Yasuhara, M., Iwatani, H., Yamaguchi, T., Yamada, K., Mamo, B., 2019. Deep-sea ostracod faunal dynamics in a marginal sea: biotic response to oxygen variability and mid-Pleistocene global changes. Paleobiology 45 (1), 85–97. https://doi.org/10.1017/pab.2018.37.

Hussain, S.M., 1998. Recent benthic Ostracoda from the Gulf of Mannar, off Tuticorin, southeast Coast of India. J. Paleontol. Soc. India 43, 1–22. https://doi.org/10.17491/cgsi/2013/63296.

Hussain, S.M., Ravi, G., Mohan, S.P., Rao, R., 2004. Recent benthic ostracoda from the inner shelf off Chennai, southeast coast of India – Implication on Microenvironments. Environ. Micropaleontol. Meiobenthol. 1, 105–121, 10.1.1.463.1696.

Hussain, S.M., Ganesan, P., Ravi, G., Mohan, S.P., Sridhar, S.G.D., 2007. Distribution of Ostracoda in marine and marginal marine habitats off and adjoining areas, southern east coast of India and Andaman Islands: environmental implications. Indian J. Mar. Sci. 36, 369–377, 10.1.146.1696.

Ikeya, N., Kato, M., 2000. The life history and culturing of *Xestoleberis hanaii* (Crustacea, Ostracoda). Hydrobiologia 419, 149–159.

Iwatani, H., Young, S.M., Irizuki, T., Sampei, Y., Ishiga, H., 2014. Spatial variations in recent ostracode assemblages and bottom environments in Trincomalee Bay, northeast coast of Sri Lanka. Micropaleontology 60 (6), 509–518.

Iwatani, H., Yasuhara, M., Rosenthal, Y., Linsley, B.K., 2018. Intermediate-water dynamics and ocean ventilation effects on the Indonesian Throughflow during the past 15,000 years: Ostracod evidence. Geology 46 (6), 567–570. https://doi.org/10.1130/G40177.1.

Jain, S.P., 1981. Recent ostracoda from southwest Kerla Coast, India. Bull. Indian Geol. Associat. 14 (2), 107–120.

Jansen, J.H.F., Kuipers, A., Troelstra, S.R., 1986. A Mid-Brunhes Climatic Event: long-term changes in global atmosphere and ocean circulation. Science 232 (4750), 619–622. https://doi.org/10.1126/science.232.4750.619.

Jellinek, T., 1993. Zur Ökologie und Systematik rezenter Ostracoden aus dem Bereich des kenianischen Barriere-Riffs. Senckenb. Lethaea 73, 83–225.

Jöst, A.B., Yasuhara, M., Okahashi, H., Brix, S., Martínez Arbizu, P., Ostmann, A., 2018. Biogeographic distributions of *Cytheropteron* species (Ostracoda) in Icelandic waters (sub-polar North Atlantic). Mar. Biodivers. https://doi.org/10.1007/s12526-018-0867-8.

Jung, S.J.A., Kroon, D., Ganssen, G., Peeters, F., Ganeshram, R., 2009. Enhanced Arabian Sea intermediate water flow during glacial North Atlantic cold phases. Earth Planet. Sci. Lett. 280, 220–228. https://doi.org/10.1016/j.epsl.2009.01.037.

Karanovic, I., Brandão, S.N., 2016. The genus *Polycope* (Polycopidae, Ostracoda) in the North Atlantic and Arctic: taxonomy, distribution, and ecology. Syst. Biodivers. 14 (2), 198–223. https://doi.org/10.1080/14772000.2015.1131756.

Karanovic, I., Tanaka, H., 2013. Ostracod genus *Parapolycope* (Crustacea): Diversity, distribution, and phylogeny, with description of the first representative from Korea. Zool. Anz. 253 (21), 35. https://doi.org/10.1016/j.jcz.2013.08.002.

Kingma, J.T., 1948. Contributions to the knowledge of the young Caenozoic Ostracoda from the Malayan region. Geologisch Instituut Utrecht, pp. 1–120.

Kondo, H., Toyofuku, T., Ikeya, N., 2005. Mg/Ca ratios in the shells of cultured specimens and natural populations of the marine ostracode *Xestoleberis hanaii* (Crustacea). Palaeogeogr. Palaeoclimatol. Palaeoecol. 225 (1–4), 3–13. ISSN 0031–0182. https://doi.org/10.1016/j.palaeo.2004.05.026.

Kunkelova, T., Jung, S.J.A., de Leau, E.S., Odling, N., Thomas, A.L., Betzler, C., Eberli, G. P., Alvarez-Zarikian, C.A., Alonso-García, M., Bialik, O.M., Blättler, C.L., Guo, J.A., Haffen, S., Horozal, S., Inoue, M., Jovane, L., Kroon, D., Lanci, L., Laya, J.C., Hui Mee, A.L., Nakakuni, M., Nath, B.N., Niino, K., Petruny, L.M., Pratiwi, S.D., Slagle, A. L., Su, X., Swart, P.K., Wright, J.D., Yao, Z., Young, J.R., Lindhorst, S., Stainbank, S., Rueggeberg, A., Spezzaferri, S., Carrasqueira, I., Hu, S., Kroon, D., 2018. A two million year record of low-latitude aridity linked to continental weathering from the Maldives. Progress in Earth and Planetary Science 5, 86. https://doi.org/10.1186/s40645-018-0238-x.

Lachkar, Z., Lévy, M., Smith, S., 2018. Intensification and deepening of the Arabian Sea oxygen minimum zone in response to increase in Indian monsoon wind intensity. Biogeosciences 15, 159–186.

Legendre, P., Legendre, L., 2012. Chapter 9 - Ordination in reduced space. In: Legendre, P., Legendre, L. (Eds.), Developments in Environmental Modelling. Elsevier, Amsterdam, pp. 425–520.

León, J.-F., Legrand, M., 2003. Mineral dust sources in the surroundings of the North Indian Ocean. Geophys. Res. Lett. 30 https://doi.org/10.1029/2002GL016690.

Lindhorst, S., Betzler, C., Kroon, D., 2019. Wind variability over the northern Indian Ocean during the past 4 million years – insights from coarse aeolian dust (IODP Exp. 359, site U1467, Maldives). Palaeogeogr. Palaeoclimatol. Palaeoecol. 536, 109371 https://doi.org/10.1016/j.palaeo.2019.109371.

Lüdmann, T., Kalvelage, C., Betzler, C., Fürstenau, J., Hübscher; C., 2013. The Maldives, a giant isolated carbonate platform dominated by bottom currents. Mar. Pet. Geol. 43, 326–340. https://doi.org/10.1016/j.marpetgeo.2013.01.004.

Maddocks, R.F., 1966. Distribution patterns of living and subfossil podocopid ostracodes in the Nosy Bé area, northern Madagascar. The University of Kansas Paleontological Contributions paper 12.

Maddocks, R.F., 1969a. Recent ostracodes of the Family Pontocyprididae chiefly from the Indian Ocean. Smithson. Contrib. to Zool. 7, 1–56.

Maddocks, R.F., 1969b. Revision of recent Bairdiidae (Ostracoda). Smithsonian Institution United States Natl Museum Bull. 295, 1–144. https://doi.org/10.5479/si.03629236.295.1.

Maddocks, R.F., 2013. New and poorly known species of *Neonesidea* (Bairdiidae, Ostracoda, Crustacea) from French Frigate Shoals, the Hawaiian Islands. Zootaxa 3608, 457–510. https://doi.org/10.11646/zootaxa.3608.6.3.

Maddocks, R.F., 2015. New and poorly known species of *Bairdoppilata* and *Paranesidea* (Bairdiidae, Ostracoda) from French Frigate Shoals and O'ahu, the Hawaiian Islands. Zootaxa 4059, 277–317. https://doi.org/10.11646/zootaxa.4059.2.3.

Maddocks, R.F., Wouters, K.A., 1990. *Triebelina? pustulata* Keij, 1974 from the Maldives Islands: more homeomorphy in the ornate Bairdiidae (Ostracoda). Bull. l'Institut R. des Sci. Nat. Belgique Biol. 60, 173–180.

Magurran, A.E., 2003. Measuring Biological Diversity. Wiley-Blackwell, New York.

Majoran, S., Agrenius, S., 1995. Preliminary observations on living *Krithe praetexta praetexta* (Sars, 1866), *Sarsicytheridea bradii* (Norman, 1865) and other marine ostracods in aquaria. J. Micropaleontol. 14, 96.

Malz, H., Jellinek, T., 1989. Cytherellide Ostracoden aus den E-Afrikanischen Küstengebeit. Modell-Vorstellungen zur differenzierung und phylogenetischen entwicklung. Cour. Forsch.-Inst. Senckenberg 113, 187–233.

Mazzini, I., 2004. Quaternary benthic Ostracoda from the Tasman Sea: distribution patterns within circumpolar deep-water. Boll. Soc. Paleontol. Ital. 43 (1–2), 217–224 (ISSN 0375-7633).

Mckenzie, K.G., Peypouquet, J., 1984. Oceanic paleoenvironment of the Miocene Fyansford Formation from Fossil Beach, near Mornington, Victoria, interpreted on the basis of Ostracoda. Alcheringa 8, 291–303. https://doi.org/10.1080/03115518408618950.

Mohammed, A.M., Keyser, D., 2012. Recent Ostracods from the Tidal Flats of the Coast of Aden City. Marine Biodiversity Senckenberg, Yemen. https://doi.org/10.1007/s12526-012-0112-9.

Mohammed, A.M., Al-Wosabi, M.A., Keyser, D., Al-Kadasi, W.M., 2012. Distribution and taxonomy of shallow marine Ostracods from Northern Socotra Island (Indian Ocean) - Yemen. Rev. Micropaleontol. 55, 149–170. https://doi.org/10.1016/j.revmic.2012.06.004.

Morris, E.K., Caruso, T., Buscot, F., Fischer, M., Hancock, C., Maier, T.S., et al., 2014. Choosing and using diversity indices: Insights for ecological applications from the German Biodiversity Exploratories. Ecol. Evolut. 4 (18), 3514–3524. https://doi.org/10.1002/ece3.1155.

Mostafawi, N., 1992. Rezente Ostracoden aus dem mittleren Sund-Schelf, zwischen der Malaiischen Halbinsel und Borneo. Senckenb. Lethaea 72, 129–168.

Mostafawi, N., 2003. Recent ostracods from the Persian Gulf. Senckenberg. Marit. 32 (1/2), 51–75.

Mostafawi, N., Colin, J.P., Babinot, J.F., 2005. An account on the taxonomy of ostracodes from recent reefal flat deposits in Bali, Indonesia. Rev. Micropaleontol. 48, 123–140. https://doi.org/10.1016/j.revmic.2004.12.001.

Mostafawi, N., Nabavi, S.M.B., Moghaddasi, B., 2010. Ostracods from the Strait of Hormuz and Gulf of Oman, Northern Arabian Sea. Rev. Esp. Micropaleontol. 42 (2), 243–265.

Munef, M.A., Al-Wosabi, M.A., Keyser, D., Al-Kadasi, W.M., 2012. Distribution and taxonomy of shallow marine Ostracods from Northern Socotra Island (Indian Ocean) – Yemen. Rev. Micropaleontol. 55, 149–170.

Nair, R.R., Ittekkot, V., Manganini, S.J., Ramaswamy, V., Haake, B., Degens, A.T., Desai, B.N., Honjo, S., 1989. Increased particle flux to the deep ocean related to monsoon. Nature 338, 749–751.

Nishath, N.M., Hussain, S.M., Rajkumar, A., 2015. Distribution of ostracoda in the sediments of the northwestern part of the Bay of Bengal, India - implications for microenvironment. J. Palaeontol. Soc. India 60 (2), 27–33.

Nishath, N.M., Hussain, S.M., Rajkumar, A., 2017. Ostracod biodiversity from shelf to slope oceanic conditions, off central Bay of Bengal, India. Palaeogeogr. Palaeoclimatol. Palaeoecol. https://doi.org/10.1016/j.palaeo.2017.05.004.

Oksanen, J., Guillaume Blanchet, F., Friendly, M., Kindt, R., Legendre, P., McGlinn, D., Minchin, P.R., O'Hara, R.B., Simpson, G.L., Solymos, P., Stevens, M.H.H., Szoecs, E., Wagner, H., 2018. Vegan: Community Ecology Package (R package version 2.5-2).

Pisias, N.G., Moore Jr., T.C., 1981. The evolution of Pleistocene climate: a time series approach. Earth Planet. Sci. Lett. 52 (2), 450–458. https://doi.org/10.1016/0012-821X(81)90197-7.

Poynter, J., Eglinton, G., 1990. 14. Molecular composition of three sediments from hole 717c: The Bengal fan. In: Proceedings of the Ocean Drilling Program: Scientific Results, pp. 155–161.

Poynter, J., Eglinton, G., 1991. The biomarker concept—strengths and weaknesses. Fresenius J. Anal. Chem. 339, 725–731.

Poynter, J., Farrimond, P., Robinson, N., Eglinton, G., 1989. Aeolian-derived Higher Plant Lipids in the Marine Sedimentary Record: Links with Palaeoclimate, Paleoclimatology and Paleometeorology: Modern and Past Patterns of Global Atmospheric Transport. Springer, pp. 435–462.

Purdy, E.G., Bertram, G.T., 1993. Carbonate Concepts from the Maldives, Indian Ocean. AAPG Stud. Geol. 34.

R Core Team, 2017. R: A Language and Environment for Statistical Computing. R Foundation for Statistical Computing, Vienna, Austria.

Reichart, G.J., den Dulk, M., Visser, H.J., van der Weijden, C.H., Zachariasse, W.J., 1997. A 225 kyr record of dust supply, paleoproductivity and the oxygen minimum zone from the Murray Ridge (northern Arabian Sea). Palaeogeogr. Palaeoclimatol. Palaeoecol. 134 (1–4), 149–169.

Reolid, J., Reolid, M., Betzler, C., Lindhorst, S., Wiesner, M.G., Lahajnar, N., 2017. Upper Pleistocene cold-water corals from the Inner Sea of the Maldives: taphonomy and environment. Facies 63, 8. https://doi.org/10.1007/s10347-016-0491-7.

Roberts, D.W., 2019. Labdsv: Ordination and Multivariate Analysis for Ecology. R Package Version 2.0-1. https://CRAN.R-project.org/package=labdsv.

Rodrigues, T., Voelker, A.H.L., Grimalt, J.O., Abrantes, F., Naughton, F., 2011. Iberian margin sea surface temperature during MIS 15 to 9 (580-300 ka): Glacial suborbital variability versus interglacial stability. Paleoceanography 26, PA1204.

Sarkar, S., Gupta, A., 2009. Deep-sea paleoceanography of the Maldives Islands (ODP Hole 716A), equatorial Indian Ocean during MIS 12–6. J. Biosci. 34 (5). Indian Academy of Sciences.

Sarkar, S., Gupta, A., 2014. Late Quaternary productivity changes in the equatorial Indian Ocean (ODP Hole 716A). Palaeogeogr. Palaeoclimatol. Palaeoecol. 397, 7–19. https://doi.org/10.1016/j.palaeo.2013.12.002.

Schlager, W., Reijmer, J.J.G., Droxler, A.W., 1994. Highstand shedding of carbonate platforms. J. Sediment. Res. B64, 270–281.

Schulte, S., Rostek, F., Bard, E., Rullktter, J., Marchal, O., 1999. Variations of oxygen minimum and primary productivity recorded in sediments of the Arabian Sea. Earth Planet. Sci. Lett. 173, 205–221.

Shin, C.P., Yasuhara, M., Iwatani, H., Kase, T., Fernando, A.G.S., Hayashi, H., Kurihara, Y., Pandita, H., 2019. Neogene marine ostracod diversity and faunal composition in Java, Indonesia: Indo-Australian Archipelago biodiversity hotspot and the Pliocene diversity jump. J. Crustac. Biol. 2019, 1–9. https://doi.org/10.1093/jcbiol/ruy110.

Simpson, E.H., 1949. Measurement of diversity. Nature 163 (4148), 688. https://doi.org/10.1038/163688a0.

Sreevidya, E., Sijinkumara, A.V., Nath, B.N., 2019. Aragonite pteropod abundance and preservation records from the Maldives, equatorial Indian Ocean: Inferences on past oceanic carbonate saturation and dissolution events. Palaeogeogr. Palaeoclimatol. Palaeoecol. 534 https://doi.org/10.1016/j.palaeo.2019.109313.

Sridhar, S.G.D., Hussain, S.M., Kumar, V., Periakali, P., 2002. Recent benthic ostracoda from Palk Bay, off Rameswaram, southwest coast of India. J. Palaentol. Soc. India 47, 17–39.

Stainbank, S., Spezzaferri, S., De Boever, E., Bouvier, A.-S., Chilcott, C., de Leau, E.S., Foubert, A., Kunkelova, T., Pichevin, L., Raddatz, J., Rüggeberg, A., Wright, J.D., Yu, S.M., Zhang, M., Kroon, D., 2020. Assessing the impact of diagenesis on foraminiferal geochemistry from a low latitude, shallow-water drift deposit. Earth Planet. Sci. Lett. 545, 116390. ISSN 0012-821X. https://doi.org/10.1016/j.epsl.2020.116390.

Stainbank, S., Spezzaferri, S., Rüggeberg, A., Raddatz, J., de Leau, E.S., Yu, S.M., Zhang, M., Kroon, D., 2021. Monsoon and tropical climate forcing on the physicochemical and thermocline characteristics of the Maldives Inner Sea: Insights from Marine Isotope Stages 1–2 and 10–13. Paleoceanogr. Paleoclimatol. 36 https://doi.org/10.1029/2020PA004105 e2020PA004105.

Steineck, P.L., Yozzo, D., 1988. The late Eocene - recent *Bradleya johnsoni* Benson lineage (Crustacea, Ostracoda) in the Central Equatorial Pacific. J. Micropalaeontol. 7 (2), 187–199. https://doi.org/10.1144/jm.7.2.187.

Stepanova, A., Lyle, M., 2014. Deep-sea Ostracoda from the Eastern Equatorial Pacific (ODP Site 1238) over the last 460 ka. Mar. Micropaleontol. 111, 100–117. https://doi.org/10.1016/j.marmicro.2014.06.003.

Stepanova, A., Taldenkova, E., Bauch, H.A., 2004. Ostracod species of the genus *Cytheropteron* from late Pleistocene, Holocene and recent sediments of the Laptev Sea (Arctic Siberia). Rev. Esp. Micropaleontol. 36 (1), 83–108.

Swanson, K.M., Jellinel, T., Malz, H., 2005. The platycopine condition: new observations on reproduction, respiration and feeding in living,deep-sea Platycopina (Crustacea, Ostracoda). Senckenberg. Marit. 35 (2), 157–187.

Tanaka, G., 2009. Adaptive modifications of carapace outlines in the Cytheroidea (Ostracoda: Crustacea). Biol. J. Linn. Soc. 97, 810–821.

Tanaka, H., Tsukagoshi, A., Karanovic, I., 2014. Molecular phylogeny of interstitial Polycopidae ostracods (Crustacea) and descriptions of a new genus and four new species. Zool. J. Linnean Soc. 172 (282), 317. https://doi.org/10.1111/zoj.12176.

Titterton, R., Whatley, R.C., 1988. Recent Bairdiinae (Crustacea, Ostracoda) from the Solomon Islands. J. Micropalaeontol. 7, 111–142. https://doi.org/10.1144/jm.25.1.73.

Titterton, R., Whatley, R.C., 2005. Recent marine Ostracoda from the Solomon Islands. Part 2: Cytheracea, Xestoleberidae. Rev. Esp. Micropaleontol. 37 (2), 291–313.

Titterton, R., Whatley, R.C., 2006a. Recent marine Ostracoda from the Solomon Islands. Part 1: Cypridoidea, Platycopina and Cladocopina. J. Micropalaeontol. 25, 73–94.

Titterton, R., Whatley, R.C., 2006b. Recent marine Ostracoda from the Solomon Islands. Part 3: Cytheroidea: Bythocytheridae, , Cytherideidae, Krithidae, Neocytherideidae, Cytheruridae. Rev. Esp. Micropaleontol. 38 (1), 169–189.

Titterton, R., Whatley, R.C., 2007. Recent marine Ostracoda from the Solomon Islands. Part 5: Cytheroidea, Leptocytheridae. Rev. Esp. Micropaleontol. 39 (1–2), 45–62.

Titterton, R., Whatley, R.C., 2008a. Recent marine Ostracoda from the Solomon Islands. Part 4: Cytheroidea; Hemicytheridae, Thaerocytheridae. J. Micropalaeontol. 27, 13–33.

Titterton, R., Whatley, R.C., 2008b. Recent marine Ostracoda from the Solomon Islands. Part 6: Cytheroidea; Paradoxostomatidae, Pectocytheridae, Trachyleberididae. Rev. Esp. Micropaleontol. 41 (1–2), 35–74.

Tjallingii, R., Röhl, U., Kölling, M., Bickert, T., 2007. Influence of the water content on X-ray fluorescence core-scanning measurements in soft marine sediments. Geochem. Geophys. Geosyst. 8 (2) https://doi.org/10.1029/2006GC001393. Technical Brief.

Tomczak, M., Godfrey, J.S., 2003. Regional Oceanography. An Introduction. Daya Publishing House, Delhi, p. 390.

Villanueva, J., Pelejero, C., Grimalt, J.O., 1997. Clean-up procedures for the unbiased estimation of C_{37} alkenone sea surface temperatures and terrigenous n-alkane inputs in paleoceanography. J. Chromatogr. A 757, 145–151.

Westerhausen, L., Poynter, J., Eglinton, G., Erlenkeuser, H., Sarnthein, M., 1993. Marine and terrigenous origin of organic matter in modern sediments of the equatorial East Atlantic: the σ13C and molecular record. Deep-Sea Res. Part I 40, 1087–1121.

Whatley, R.C., 1991. The Platycopid signal: a means of detecting kenoxic events using Ostracoda. J. Micropalaeontol. 10 (2), 181–185.

Whatley, R., Coles, G., 1987. The late Miocene to Quaternary ostracoda of Leg 94, Deep Sea Drilling Project. Revista Española de Micropaleontología XIX (1), 33–97.

Whatley, R.C., Keeler, N., 1989. Ostracodes actuels de l'Ile de la Réunion (sud-ouest de l'Océan Indien). Rev. Micropaleontol. 32 (1), 63–84.

Whatley, R.C., Zhao, Q., 1987. Recent Ostracoda of the Malacca Straits. Part I. Rev. Esp. Micropaleontol. XIX 327–366.

Whatley, R.C., Zhao, Q., 1988. Recent Ostracoda of the Malacca Straits. Part II. Rev. Esp. Micropaleontol. XX 5–37.

Whatley, R.C., Pyne, R.S., Wilkinson, I.P., 2003. Ostracoda and palaeo-oxygen levels, with particular reference to the upper cretaceous of East Angola. Palaeogeogr. Palaeoclimatol. Palaeoecol. 194, 355–386.

Wouters, K., 1996. On the discovery of a cretaceous representative of the extant marine interstitial genus *Iliffeoecia* Maddocks, 1991 (Ostracoda, Pontocyprididdae). In: Proc. 2nd Eur. Ostracodologists Meet. Glas. 1993 1991, pp. 57–62.

Wouters, K., 1997. A new genus of the family Pontocyprididae (Crustacea, Ostracoda) from the Indian and Pacific Oceans, with the description of two new species. Bulletin de L'Institut Royal des Sciences Naturelles de Belgique, Biologie 67, 67–76.

Wouters, K., 2004. Review of the genus *Neocytheromorpha* Guan (Crustacea, Ostracoda), with the description of two new species from the Indian Ocean. Bull. l'Institut R. des Sci Nat. Belgique, Biol. 74, 49–60.

Wyrtki, K., 1973. Physical Oceanography of the Indian Ocean, the Biology of the Indian Ocean. Springer, pp. 18–36.

Yamada, K., Irizuki, T., Ikehara, K., Okamura, K., 2014. Calibration of past water temperature in the Sea of Japan based on Mg/Ca of ostracode shells of two shallow marine species in the genus *Cytheropteron*. Palaeogeogr. Palaeoclimatol. Palaeoecol. 410 (2014), 244–254.

Yasuhara, M., Cronin, T.M., 2008. Climatic influences on deep-sea ostracode (Crustacea) diversity for last three million years. Ecology 89 (11), 53–65.

Yasuhara, M., Okahashi, H., 2014. Quaternary deep-sea ostracode taxonomy of Ocean Drilling Program Site 980, eastern North Atlantic Ocean. J. Paleontol. 88 (4), 770–785.

Yasuhara, M., Cronin, T.M., deMenocal, P.B., Okahashi, H., Linsley, B.K., 2008. Abrupt climate change and collapse of deep-sea ecosystems. Proc. Natl. Acad. Sci. 105 (5), 1556–1560. https://doi.org/10.1073/pnas.0705486105.

Yasuhara, M., Okahashi, H., Cronin, T.M., 2009. Taxonomy of Quaternary deep-sea ostracods from the western North Atlantic Ocean. Palaeontology 52, 879–931.

Yasuhara, M., Hunt, G., Cronin, T.M., Hokanishi, N., Kawahata, H., Tsujimoto, A., Ishitake, M., 2012. Climatic forcing of Quaternary deep-sea benthic communities in the North Pacific Ocean. Paleobiology 38, 162–179.

Yasuhara, M., Stepanova, A., Okahashi, H., Cronin, T.M., Brouwers, E.M., 2014. Taxonomic revision of deep-sea Ostracoda from the Arctic Ocean. Micropaleontology 60, 399–444.

Yasuhara, M., Iwatani, H., Hunt, G., Okahashi, H., Kase, T., Hayashi, H., Irizuki, T., Aguilar, Y.M., Fernando, A.G.S., Renema, W., 2017. Cenozoic dynamics of shallow-marine biodiversity in the Western Pacific. J. Biogeogr. 44, 567–578.

Zhao, Q., Wang, P., 1990. Modern ostracoda in shelf seas off China: zoogeographical zonation. Oceanologia et Limnologia Sinica 21 (5), 458–466 (In Chinese).

Zhao, Q., Whatley, R.C., 1989. A taxonomic revision of the new species of ostracoda described by J.T. Kingma (1948) from the late Cainozoic of Indonesia. Acta Micropalaeontologica Sinica 6 (3), 229–246.

Zhao, Q., Whatley, R.C., 1997. Distribution of *Krithe* and *Parakrithe* in bottom sediments of the East China and Yellow Seas. Mar. Micropaleontol. 32, 195–207.

Zhao, Q., Zheng, L., 1996. Distribution of deep-sea ostracods in bottom sediments of the South China Sea. Acta Oceanol. Sin. 18 (1), 61–72 (In Chinese).

Zhao, Q., Whatley, R.C., Zhou, B., 2000. The taxonomy and distribution of recent species of the ostracod genus *Cytheropteron* in the South China Sea. Rev. Esp. Micropaleontol. 32 (2), 259–281.